THEORETICAL AND EXPERIMENTAL INVESTIGATIONS INTO THE EROSION RATES IN EDM PROCESS

by

RAM KUMAR

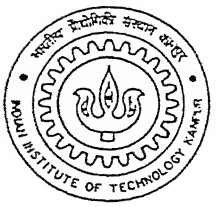

to the

DEP TMENT OF MECHANICAL ENGINEERING
INI AN INSTITUTE OF TECHNOLOGY, KANPUR

April, 2 0 0 0

CERTIFICATE

This is to certify that the work presented in the thesis entitled " ***Theoretical and Experimental Investigations into the Erosion Rates in EDM process***", has been carried out by Ram Kumar (Roll No. 9810530) under my supervision and that this work has not been submitted elsewhere for a degree.

April, 2000

Dr. M.K.Muju
Professor
Department of Mechanical Engineering
Indian Institute of Technology
Kanpur – 208016

Acknowledgement

It is my proud privilege to express my deep sense of gratitude and indebtedness towards my thesis supervisor Dr. M. K. Muju for his excellent supervision, skilled guidance, stimulating discussions and constant encouragement, which were the vital factors in successful completion of the present work. I am heartily thankful to him for the confidence he showed in me.

I am thankful to the staff of Manufacturing Science Laboratory, Mr. R. M. Jha, Mr. H. P. Sharma, Mr. Namdeo and Mr. Anil for their consistent effort and cooperation during the course of experiments carried out in the lab.

I thankfully acknowledge to all faculty members of I.I.T. Kanpur who have taught me various courses during my academic program.

I am thankful to Mr. N. K. Jain and Mr. Vinod Yadav for their constant encouragement and invaluable suggestions. I would like to express my thanks to all who helped me, especially Mr Phoolchand and Raj Kumar of Mechanical Work Shop.

I would also like to cherish the nice company of my friends Om Prakash, Ravindra, Sudhir, Satyaveer (Kodhi), Anant, Dharmendra, Kesri, Baitha, Benu and Santosh for their timely help and friendly cooperation in sorting out my problems and making my stay at I.I.T. Kanpur, a pleasant and memorable one.

Last but not the least, I would like to thank almighty God and my family members who made me to reach this stage, where I could undertake the work of this magnitude.

Ram Kumar

CONTENTS

List of Figures

List of Tables

ABSTRACT

In the present work, investigation has been done experimentally as well as theoretically to study the effect of electrode material, polarity and dielectric medium on the performance of EDM process. Theoretical crater volume for cathode and anode has been evaluated by using experimentally obtained equivalent crater volume in Pointed Heat Source Model (PHSM) for the *cathode erosion* and Expanding Circular Heat Source Model (ECHSM) for *anode erosion* respectively. In both models consideration has been taken that the fraction of energy going to the electrode is a function of energy input with some logical justification. Eleven sets of electrode pairs have been selected from the list of electrode material of Copper, Mild-Steel, Graphite and Titanium.

It has been observed that the material removal rate of cathode is always more than anode for the similar material electrode pairs. It is observed that the erosion rate from cathode of MS, Cu and Ti gives always higher erosion rates when copper is used as anode in comparison to MS and Ti anodes. This shows that copper anode is showing special characteristics in controlling the cathode erosion as compared to others. A very significant feature of huge difference in the sum of the erosion rates of dissimilar electrode pair has been observed by interchanging their polarity. It has also been observed that the new dielectric ITW (company name) gives better erosion rates than kerosene.

Finally it is concluded that distribution of energy per pulse to the tool electrode, workpiece and dielectric and hence the erosion rates depend significantly on the electrode material pairs, polarity of the electrodes as well as dielectric medium.

NOMENCLATURE

a, b, c : Constants in the average discharge current equation

C_p : Specific heat $(J/Kg\ ^oK)$

E : Total energy input at the inter-electrode gap (J)

ECHSM : Expanding Circular Heat Source Model

f : Fraction of power lost

Gr : Graphite

ITW : Company name of new dielectric

I : Average discharge current (amp)

K_T : Thermal conductivity $(W/m\ ^oK)$

MS : Mild-Steel

PHSM : Pointed Heat Source Model

q_o : Heat flux (W/m^2)

r : Radius of melt front

r_g : Effective radius

R : Radius of equivalent crater at melting temperature(T_m)

T : Temperature (^oK)

Ti : Titanium

t : Time(μsec)

t_{off} : Pulse off time (sec)

t_{on} : Pulse on time (sec)

U : Discharge voltage $(Volts)$

V : Crater volume (mm^3)

$\dot{V}_w$: Volumetric erosion rate (mm^3/min)

WTER : Work-Tool Erosion Ratio $\left[\dfrac{\text{Erosion rate of work(cathode)}}{\text{Erosion rate of tool (anode)}}\right]$

z : depth or axial coordinate

Greek symbols

α : Thermal diffusivity (m^2/sec)

ρ : Density (Kg/m^3)

Subscripts

a	: related to anode
c	: related to cathode
d	: dielectric
e	: electrode
m	: melting conditions
o	: ambient conditions
off	: pulse off
on	: pulse on
r	: radiation
w	: workpiece

Superscript

'	: MS(-ve)/Cu(+ve) system
''	: Cu(-ve)/MS(+ve) system

Chapter 1

INTRODUCTION

1.1 Introduction

Electric discharge machining (EDM) sometimes referred, as Electric spark machining is a thermoelectric process in which heat energy of a spark is used to remove material from the workpiece. The workpiece and tool should be made of electrically conductive materials. A spark is produced between the two electrodes (tool and work-piece) in the presence of dielectric fluid and its location is determined by the narrowest gap between the two surfaces. The spark wanders in a random manner all over the surface. Duration of each spark is very short. The entire cycle time is usually few micro-seconds (μs). The frequency of sparking may be as high as thousands of sparks per second. The area over which a spark is effective (or spark radius) is also very small. However, temperature of the area under the spark is very high. As a result, the spark energy is capable of partly melting and partly vaporizing material from localized area on both the electrodes, i.e. workpiece and tool. The material is removed in the form of *craters* that spread over the entire surface of the workpiece. Finally, the cavity produced in the workpiece is approximately the replica of the tool. To achieve an effective material removal in a controlled manner presence of a suitable dielectric fluid between the electrode and work material and a direct current power source are important elements of the process.

The dielectric medium plays an important and complex role in metal removal. It keeps the discharge zone confined to a narrow channel, cools the electrodes and carries the products of discharge (debris) away from the machining zone. The type, quality and flushing arrangement of the dielectric also influences the generated surface.

The process is of great utility in machining very hard and tough metals and alloys including ceramics. Although both the electrodes get eroded, the operating

parameters and polarity should be selected carefully, so as to limit the wear of tool electrode to about one percent or less of the work-piece erosion.

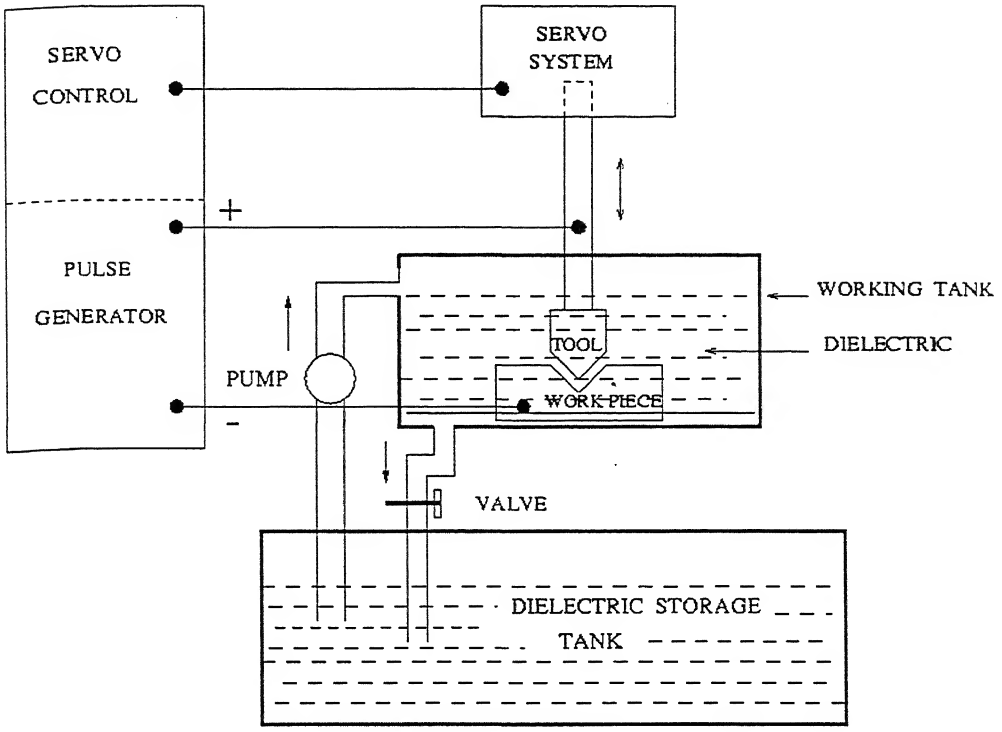

Fig 1.1: Schematic diagram of EDM process.

Fig.1.1 shows the basic scheme of the process. In resistance and capacitance type of the circuit an applied voltage of about 200 *Volts* across a typical gap of 20 to 40 μm causes the dielectric to breakdown. The voltage falls to about 25 *Volts* after the breakdown. Using the servo-controlled feed of the tool electrode to maintain a small working gap can stabilize the required discharge conditions. In this situation the forming electrode (tool) reproduces shape upon the workpiece. It is observed that polarity determines the rate of material removal. When the pulse duration is very small, typically less than 1 micron, the positive electrode erodes faster than the negative electrode. But for longer pulse durations it is the negative electrode, which erodes faster. And this is true even for similar materials with some exceptions. For this reason in die-sinking machines the work is connected to negative electrode while in wire EDM machines the wire is connected to the negative terminal of the D.C. supply. This aspect of polarity is discussed later.

1.1.1 Pulse Generation

The type of pulse generation system selected for EDM for the purpose would essentially depends upon the application.

(i) Low energy range systems: Low energy range systems are selected when the objective is to remove small amounts of material as in finishing operations. Resistance-capacitance relaxation circuits with a constant D.C source represent this class. Supply voltages used range from 100 to 500 *Volts* and peaks currents are upto 1000 *amps*. The breakdown voltage (V) and the capacitance (C) determine energy supplied to the gap between electrode.

The pulse form and pulse time depend upon the impedance of the discharge circuit, including capacitor and there is little control that can be exercised. In these systems the charge cycle is long compared to discharge time which result in low time utilization of the cycle, hence low efficiency. Also the half wave can lead to increased tool wear. Since material removal rate with these circuits is low, these systems have preferential use in finishing applications.

(ii) High energy range systems: These systems are selected for medium and rough machining and controlled pulse generators are used for this type of machining. In controlled pulse generators, pulse duration and repetition time can be selected and controlled independent of the spark conditions leading to more efficient time utilization. The characteristics typical pulse generator circuit is shown in Fig.1.2. Also Fig.1.3 shows the types of pulses obtained in EDM using these machines.

In these generator energy from a D.C source ($60 - 20\ V$) is supplied to the working gap via resistor and electronic switch. The power supply voltage, arc voltage and the resistor determine the magnitude of the current level. Currents range from 1 *amp* to 100 *amp* Pulse times obtainable are in the range of 0.1 *microsec* to several *millisecs*. The pulse shape is usually rectangular. The relative tool wear is kept low by utilizing suitable pulse time-pulse current ratios. A non-rectangular pulse like a trapezoidal one results in very low relative tool wear. Controlled pulse circuits provide an important feature of automatic stoppage of current flow when a short circuit occurs.

Discharge pulses produced by generators as against those from relaxation circuits are unidirectional and hence don't have disadvantages of revere material

removal. Thus, tool wear is inherently less. This leads to improved reproduction accuracy and higher material removal rates.

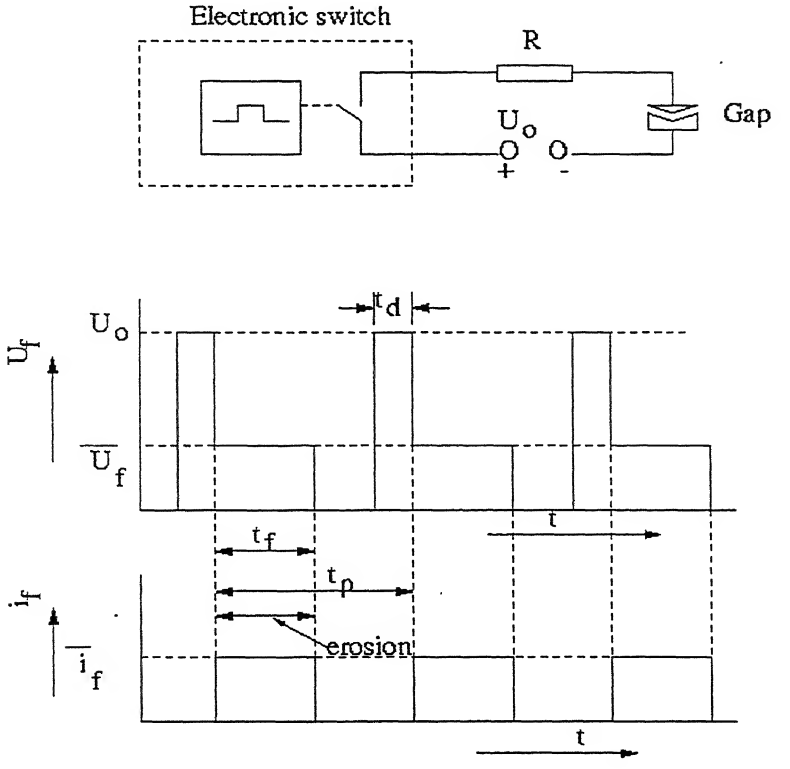

Fig 1.2: Characteristic of a typical pulse generator.

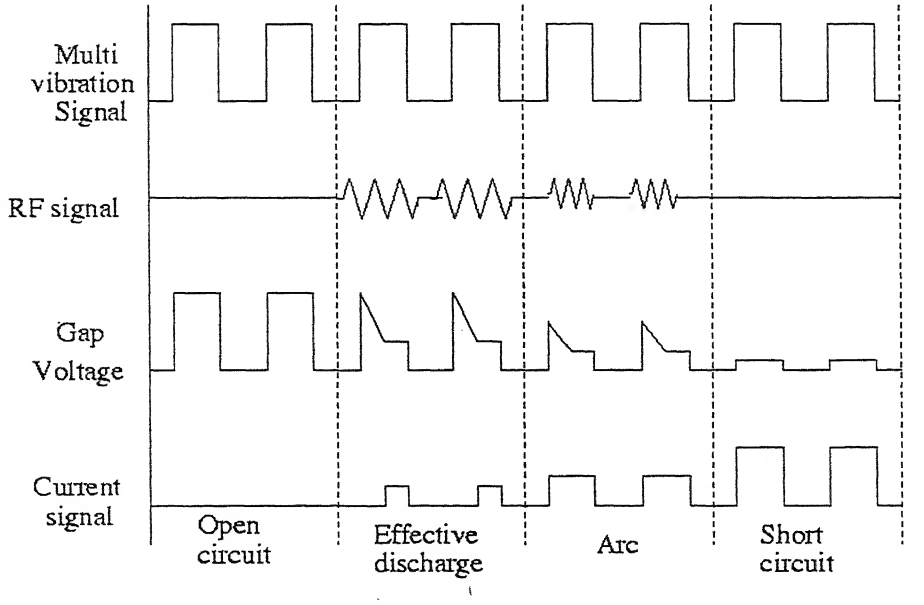

Fig 1.3: Types of pulses in EDM.

1.1.2 Spark Frequency

While an arc is a stable thermionic phenomenon, a spark is a sudden transient and noisy discharge between two electrodes. The latter situation occurs in EDM process. Discharge of approximately 1 *micro-sec* to 1 *milli-sec* are encourages in EDM process. Shorter duration sparks have less energy and consequently remove less material and give better surface finish. However, if the ratio of the pulse duration (t_{on}), also called as on-time, to pulse cycle time (t_c) is increased, probability of arcing is seen to increase, especially for the low values of pulse duration. Hence, to avoid arcing, pulse cycle time should be increased. This implies is that sufficient time needs to elapse before the dielectric quenches the spark and is ready for the next spark. Arcing can also be avoided by periodically widening the working gap to facilitate flushing.

1.1.3 Changing from sparking to arcing

Sparking is the ideal machining condition as it gives controlled erosion of work-piece. It is a condition in which several successive sparks are formed each time a voltage pulse is successfully discharged across a gap. These sparks occurs in rapid succession and in randomly changing positions resulting in fairly uniform material removal.

Arcing on the other hand is one heavy discharge of energy lasting for most of the pulse time. This is concentrated in one place to give uncontrolled erosion, which can severely damage work-piece and electrode. With arcing it is impossible to get good surface finish. Trapezoidal pulse waveform is found to be more efficient than rectangular. However, the latter being easier to produce are more commonly employed. A trapezoidal pulse in which the current is large at the beginning and declines linearly produces a crater volume for a single spark that is almost three times that obtained with the standard rectangular pulse. Conversely, using a pulse with higher current towards the end, machining rate is lower while electrode wear is also lower and the surface finish is better. Therefore design of an optimum pulse profile is of research and application interest.

1.1.4 Plasma region

In a typical EDM operation discharge occurs across a narrow gap between the two electrodes when field strength of about 10,000 *V/mm* to 100,000 *V/mm* is established. Discharge, however, occurs only some time after the supply voltage is impressed across the electrodes. This delay is referred to as *ignition-delay*. Electric field between the electrode tends to increase when the voltage across them is increased and gap is decreased. When the field reaches to a certain level electrons get emitted from the cathode. The emitted electrons together with any available in the gap are accelerated by the applied field. The newly generated electrons and ions also get accelerated towards the anode and cathode respectively causing further ionization and the chain reaction occurs producing an avalanche of ions. The region in which this avalanche occurs is called *plasma channel*. Fig1.4 is a schematic diagram showing the plasma region.

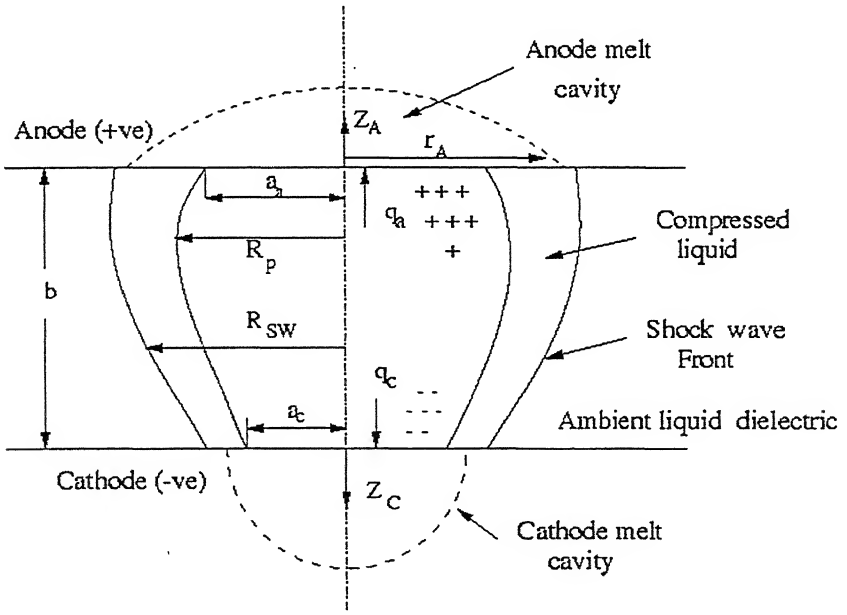

Fig 1.4: A schematic diagram of the EDM process showing the circular heat source, plasma configuration, and melt cavities after a certain On-time.

The situation in the plasma channel is complex with fast moving electrons, ions and neutral particles all interacting under electrostatic forces and collision. Some atoms and ions are excited by collision leading to emission of light. Part of this light is used in the photo-ionization of neutral particles, the rest enables the spark to be seen. A

plasma channel, surrounded by a vapor bubble grows during the on-time which is usually less than 100 *microsecs*. The surrounding dense liquid dielectric restricts the plasma growth. Input energy (UIt_{on}) is thus concentrated in a very small volume. The local plasma temperatures as high as 40,000 K are reached. Dynamic plasma pressure rises to be as high as 3 *kbar* due mainly to inertial (density) effects. Viscosity effects are thought to be responsible for the plasma shape of Figure 1.4.

1.1.5 Mechanism of Discharging

The removal of material in electrical discharge machining is based upon the erosion effects of electric discharges occurring between two electrodes. The discharge mechanism can be explained by dividing it into different phases and stages.

The first phase, known as the preparatory phase, is only for a very limited time (10^{-7} to 10^{-8} seconds for a discharge of 4 to 6 $\times$ 10^{-6} seconds). During this phase, the powerful electric field ionizes the dielectric medium and thus forms high conductivity channel. The second phase is characterized by the discharge itself in the form of heavy flow of current similar to an avalanche of electrons. The third phase is the injection of the eroded metal, which may start during the second phase and may continue even after the end of discharge. These three phases can be represented by the stages shown in Fig 1.5.

The intensification of the electric field between the most closely situated peaks of electrode surfaces causes the polarization, as well as orientation, of the molecules and ions of the dielectric medium, as shown in Fig1.5a.

As this polarization reaches a certain level, the negative and positive streamers organize and open the way to the current, as shown in Fig1.5b. As the resistance of the dielectric medium reaches very high values (10^7 to 10^8 *A/sec*). This ionized channel consists of plasma formed with positive ions and free electrons, and with the vapor of metals constituting both electrodes, and with gas resulting from the chemical decomposition of the dielectric under the effect of the electric spark as illustrated in Fig1.5c. The flow of high-intensity current ionizes still further the discharge channel and produces a strong magnetic field, which attracts the ions towards the axis of the discharge channel. These ions compress the current beam causing addition heating of channel which may be significantly greater than 10,000° C. This quantity of heat is

sufficient to melt a certain volume of metal and even to evaporate part of this volume, as shown in Fig1.5d.

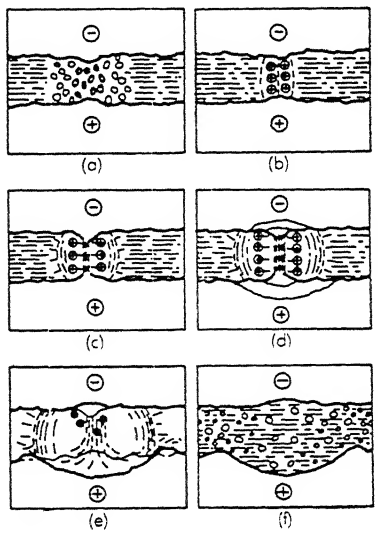

Fig 1.5 Successive stages of discharging in EDM process.

The ejection of the melted and evaporated metal leaves specific marks on the edges of the crater, as illustrated in Fig1.5e. One can see the characteristic crater appearing on the anode as well as similar crater on the cathode in Fig1.5f. After the pulse-on period is over, the dielectric with the gap deionises completely and the channel of electrical conductivity ceases to exist. A fresh discharge may initiate between the tool and work electrodes at some other points at which the asperties of electrodes are at their closest.

The following are features of EDM process have been visualized:

i) During the pulse on-time the high energy plasma melts both the electrodes by conduction, but limited electrode vaporization occurs due to high plasma pressure.

ii) Anode first melts rapidly due to absorption of fast moving electrons at the start of the pulse, but then begins to resolidify after a few microseconds. This is

thought to be due to expansion of plasma radius at the anode resulting in decrease in local heat flux at the anode surface.

iii) Melting of the cathode is delayed in time by one or two orders of magnitude beyond that of the anode due to lower mobility of positive ions.

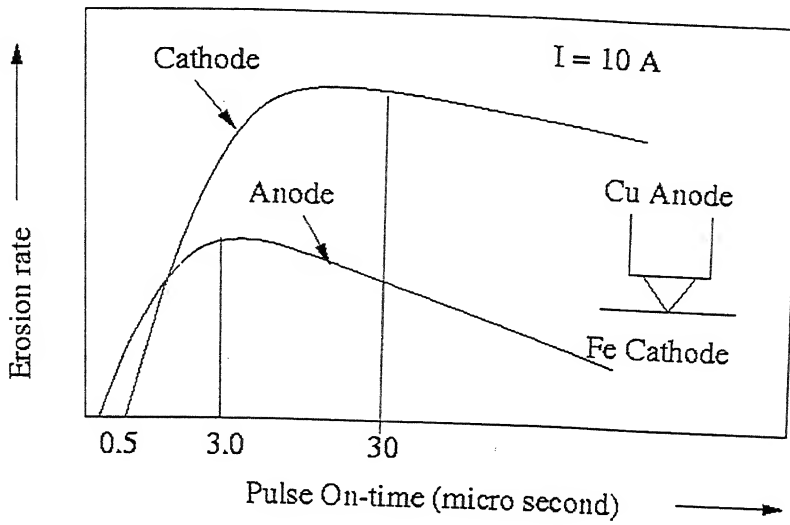

Fig 1.6:The difference between anode and cathode erosion rates with different On-time (not to scale)

iv) Since cathode is emitting electrons the plasma radius at the cathode is also much smaller, thereby approximating a pointed heat source for conduction into its interior.

v) The current density decreases strongly with the increasing depth beneath the electrode surface. Hence the temperature rise in the electrodes due to joule heating is found to be negligible.

vi) At the end of on-time (t_{on}), pause time (t_{off}) begins when power is terminated to the machine. During this time a violent collapse of the plasma channel and vapor bubble occurs, causing the superheated, molten liquid on the surface of both the electrodes to explode into the liquid dielectric. This leaves cavities of usually less than 100 μm in width on the electrodes thus leaving an ultra-smooth finish.

vii) Fig 1.6 shows how the erosion rate of curves for the cathode and anode cross over at about 0.5 μs, for particular case.

viii) For die-sinkers the cathode is usually the work-piece and anode the shaping tool. The optimum pulse times of 10 to 100 μ *secs* are used.

ix) For such long on-times, anode erosion is low due to resolidification.

1.2 Literature Review

The phenomenon of metal removal by EDM process is quite complex to analyze. This is on account of the facts that a number of interdependent variables have a controlling effect on the process. Several researchers have considered the physical events during EDM process and provided explanations to the discharge and erosion phenomenon [3,7,8,12,14,22,35,40]. Mathematical modeling of the process is generally done on the basis of isolated single sparks [5,6,16,22,26,28,30,33,34].

Heuvelman et al. [16] have conclusively shown that the breakdown mechanism of a liquid is not caused by collision ionization of the liquid molecules as the mean free path in liquids is comparatively small. They have also shown that the ignition delay strongly depends on the energy per unit volume added to gap, which implies that the ignition delay strongly dependent on the gap width. Thus they suggested that it would be better to use the ignition delay as a sensor for the servo-system instead of the voltage drop across the electrodes. Eubank et al. [10] have shown quantitatively that superheating is the dominant mechanism responsible of spark erosion in EDM process. Violent forces associated with superheating are the strong enough to separate small molten cavities from solid metal to form the crater.

Soneys et al. [39] have found a fairly good correlation between the sum of the discharge duration per second and the material removal rate. Guerrero-Alvarez et al. [14] have studied the electro erosion phenomenon of *Fe* and *Zn* by SEM analysis. They found that the volume of metal removal from cathode was larger than that from the anode irrespective of the discharge energy and electrode material. Cross deposition from cathode to anode in all samples was larger than the cross-deposition from anode to cathode, independent of energy and material.

Marty [26] has described a thermal model with non-dimensional analysis for the spark erosion process and obtained a series of datas relative to electrode wear, heat source radius, crater shapes by using general function. Dharmadhikari et al. [4]

have discussed a more realistic thermal model in which a finite number of heat sources distributed over work and tool surfaces. They observed that multiple source model is to be more accurate than the single source model. For a certain value of number of heat sources (N=13), the material removed per pulse computed by the proposed model, almost completely matches with the experimental results for values of pulse on time beyond 50 μsec.

Vaseekaran et al. [40] have studied the spark erosion in TiB_2 and Zn on the basis of the effects of the tool geometry, input energy and electrode polarity.
Longfellow et al. [25] have studied the behavior of electrode material properties on the wear ratio experimentally. They have postulated that the intrinsic physical properties of the electrode material that govern the wear ratio are

(i) Cohesive energy.

(ii) Mechanical strength and toughness.

(iii) Ratio of evaporation temperature (^oK) to melting temperature (^oK) and

(iv) Electrical resistivity.

The electrode of low resistivity would absorb less thermal energy from resistance heating than one of high resistivity, thereby making available addition energy for heat generation and subsequent erosion of material from the workpiece.
They established a relation for *wear ratio* (W.R) in terms of *cohesive energy* of two electrodes for some electrode pair.

At low pulse times it has been postulated that electrical forces are responsible for the material removal [8,22,38,40]. However studies at high pulse times shows that thermal properties are more effective than mechanical properties in the EDM process and the predominant thermal phenomenon is vaporization, rather than melting [8,14,22,25,40]. Depending on the discharge condition and the material, 10-15% of the final crater volume vaporizes [7,8]. The molten material cannot be removed completely because of surface tension, tensile strength and bonding forces between the liquid and solid phase [8,40]. Singh et al [38] have proposed a thermo-electric model for calculating the electrostatic forces on the surface of the cathode and the stress distribution inside the metal during a discharge. And their model suggests that the electrostatic forces are the major cause of metal removal for short pulses and the melting becomes the dominant phenomenon for the long pulses.

Guerrero-Alvarez et al. [14] have observed a decrease in removal efficiency at higher energy. This is explained on the basis of electrode gap spacing, which increases at higher energies in order to maintain the breakdown field constant. As the length of the discharge column is increased, the amount of heat loss, the radial diffusion of ions, and recombination occurring between the anode and cathode drop region also increases. Hence the removal efficiency decreases at higher energies.

George et al. [12] and Albinski [19] have suggested that in order to increases the work erosion rate, the polarity of electrodes has to be determined experimentally, which depends on tool material, work material, area and pulse length combination. Heng et al. [15] have proposed a new kind of pulse waveform, known as the polarity-change pulse. The workpiece polarity was change from positive to negative without allowing plasma extinction during the discharge. He observed greater workpiece removal rate and smaller tool erosion rate. Erden et al. [7] have indicated that for different pulse durations, there may be different optimum pulse shapes.

Many authors [8,12,40] have studied the effect of debris concentration on erosion and electrode wear. Vaseekaran et al. [40] have reported that debris tend to move into the discharge channel under the influence of electric field in the gap, leading to rapid fluctuation in the resistance. Erden [8] has observed that addition of metal powders *like Al,* Cu and Fe in Kerosene dielectric increases erosion rate of both tool and workpiece. However carbon usually results in decrease in the erosion rate. George et al. [12] have observed a higher amount of tool (anode) wear with clean dielectric compared to unfiltered and contaminated liquid. Jaswani [17] had observed experimentally that the addition of 4 *g* of fine graphite powder (10 μm of average size) per litre of kerosene increases the metal removal rate by 60 % and the tool wear rate by 15 % in EDM process. The wear ratio is reduced by about 28 %. This is due to reduction in the breakdown voltage of kerosene dielectric caused by addition of the graphite.

Jaswani [18] had compared the performances of kerosene and distilled water as a dielectric and found that distilled water resulted in higher erosion rate and lower wear ratio than in kerosene when high pulse energy range (72 – 288 *mJ*) was used. Jilani et al. [21] had reported the machining characteristics of distilled water, tap water and mixture of 25% tap and distilled water when used as a dielectric fluid. They

had found that the best machining rates have been achieved with tap water and given a suitable reason for that.

Study of the effect of dielectric composition on the machining rate [23] has shown that in general with other condition is equal, the lowest material removal rate is obtained with oils. It has also been observed that a high efficiency is achieved with Kerosene and it is increased even more with light alcohol and some other derivatives of benzene. Thermal capacity of the dielectric fluid is responsible to alter the proportion of heat transmitted through the electrode and hence influence the erosion and erosion ratio of the electrodes.

Lonardo et al.[24] have evaluated the effect of electrode material and flushing, in conjunction with electrode wear and surface quality through a complete factorial experiments. The analysis has considered separately roughing and finishing regimes, by adopting the operative conditions usually recommended in industrial production.

George et al. [11] have observed a reduction in machining rate with the use of dielectric flushing. However Snoeys et al. [39] have observed almost no effect of dielectric flushing on the material removal rate. Konig et al. [22] have reported that the energy stored in a dielectric fluid follows a curve similar to sum of erosion rate and wear rates. Erden et al. [9] have examined and compared eight different thermo-mathematical models for electrode erosion by different researchers.

Some researchers have studied the energy distribution at the electrodes. It has been reported that the fraction of power going to cathode depends on the pulse shape, current, pulse duration and type of machining i.e., rough or fine [7,8,22]. Erden [8] has reported that the fraction of power going to cathode depends on the work function of the material and some extend on its atomic weight. Shankar et al. [37] have proposed that percentage of input heat going to cathode, anode and dielectric stabilizes after a small fraction of pulse time. However, DiBitonto et al. [5] and Patel et al. [34] have considered the fraction of power going to an electrode is nearly constant for a particular electrode in a particular dielectric liquid and is independent of current and pulse time.

1.2.1 Present states of theoretical models for estimation of erosion rates

Many of the researchers have attempted to model the EDM process to estimate the erosion rates and were successful at varying degrees. Some of these are discussed below.

Dick et al. [6] obtained the crater volume in EDM by numerically solving a thermal model. The computational procedure was based on the exact solution of the related two-dimensional transient heat conduction problem in a finite or semi-infinite body subjected to a stepwise or time-dependent uniform flux over a small circular part of its upper surface. It is shown that theoretical model should include the possibility of accounting for the plasma channel widening in order to obtain acceptable agreement with experimental data or to predict the optimal operating conditions.

Pandit et al. [31,33] Modeled EDM process from surface roughness profiles by using data dependent system approach. This method bridges the gap between single discharge approach and the time – averaged approach by defining and obtaining a "characteristic crater" from EDMed surface profiles. The characteristic crater accounts for the randomness of the process and includes the effect of mutual interactions and successive dependencies within a train of discharges in the practical domain of electric-discharge machining.

Pandit et al. [32] have applied the Data Dependent System technique (DDS) to thermal modeling by developing a transient temperature distribution for the EDM process. An equation to the melting isothermal curve is defined from the DDS model obtained from readily measurable surface profiles of actual machined surface created by the random superposition of electric discharges. This equation is then combined with the heat conduction equation, to develop a transient temperature distribution.

Shankar et al. [37] have proposed a model treating discharge process and temperature distribution in the electrodes and dielectric together by employing the finite element method. The spark profile in terms of the spark radii at different cross-section has been shown different which is found to be non cylindrical with the smallest cross-section occurring at the middle of a discharge. They explained the profile on the basis of the variation of electrical conductivity with temperature.

McGeough et al. [28] developed a macroscopic model based upon the assumption that the time dependent electric field can be replaced by an electrostatic field, and the experimental observation that the dielectric breakdown process would start only if the electric field is more than a critical value. They also assumed that the material removal from tool and work-piece is proportional to the energy transmitted by the spark. The overall shapes of the tool and work-piece were determined by solving the Lapace equation of electric potential.

Later Pandey and Jilani [19,20,30] have calculated the crater volume by modifying the two-dimensional disk heat source model by accounting for the growth of the plasma channel during the pulse on-time. This consideration has led to a marked improvement in the results and correspondence between the theoretical and experimental data. The analytical results also demonstrate the effect of electrode material on the rate of plasma channel growth. This model also enables one to obtain the thickness of heat-affect zone and the extent of thermal damage suffered by the electrode material due to a single spark with a fair degree of accuracy.

A detail modeling was adopted by DiBitonto et al.[5] and Patel et al.[34] to find out the material removal rate from both the anode and cathode. Separate models for cathode and anode erosion were considered. These models are largely based on the actual experimental observations of previous researchers on sparking phenomenon in closed chambers. *Expanding circular heat source model (ECHSM) was developed for anode erosion and pointed heat source model (PSHM) for the cathode erosion.* These two models are taken into account the fraction of power distributed between two electrodes, which in-turn depends upon the electrode materials and dielectric fluid. Therefore *these model takes into the consideration the effect of dielectric and the effect of one electrode material over the erosion rate of the other electrode.*

In the present work, pointed heat source model (PHSM) [5] for cathode erosion estimation and expanding circular heat source model (ECHSM) [34] for anode estimation are considered, for some similar and dissimilar tool and electrode material pair.

1.3 Objective and scope of the present work

In EDM process, there is erosion of both work and tool. For the same material of tool/work combination the difference in erosion rates of electrodes depends on polarities of electrodes. Also there is significant difference in the sum of erosion rates of electrodes in dissimilar tool and work electrode pairs by interchanging the polarity. Hence an important consideration in EDM is to choose a suitable polarity of the electrodes in order to minimize the erosion of tool.

The objective of the present work was therefore, chosen:

1. To examine the ratio of work and tool erosion rates for similar and dissimilar pairs with pulse on-time variation.
2. To verify the applicability of pointed heat source model (PHSM) for cathode erosion estimation with similar and dissimilar tool/work electrode pairs.
3. To verify the applicability of expanding circular heat source model (ECHSM) for anode erosion estimation with similar and dissimilar tool/work electrode pairs.
4. To examine the variation of the sum of tool/work erosion rates of dissimilar electrode material pairs with the interchange of their polarity, and
5. To investigate the effect of anode materials on the erosion rate of cathode.

Chapter 2

EXPERIMENTAL OBSERVATIONS

2.1 Experimental Setup

A series of experiments were conducted on die-sinking type EDM machine [*Model Elektra R-35 and R-50 ZNC* Electronic M/C tools Limited, Pune, India) equipped with a solid state power supply. The base unit of the machine supports the discharge cell that contains the dielectric and the fixture to hold the work-piece. A continuous flow of the dielectric was maintained by pump. The work-piece was mounted on the suitable fixture. The tool electrode was mounted in a collet. Longitudinal feed of the tool electrode was maintained with a servo-motor. The inter-electrode gap was maintained constant with the servomotor. An electronic weighing machine "Afcoset" (l.c.=1mg) was used to measure the weight of the tool electrode and work-piece.

During the trial of the experiments it was observed that average current during discharge varies with pulse On-time. The variation is much at the low pulse time, however it remains almost constant for the higher pulse times. In the present study, average current for each particular pulse time was estimated and has been considered as a dependent parameters.

2.2 Test and Measurement Procedure

The tool electrode was always connected to positive terminal and the work-piece to the negative terminal for each experiment. Side flushing was done to remove the debris from inter-electrode gap and hence avoid possible short-circuiting.

Following were the test conditions used:

Tool size and shape: *5 mm* diameter cylindrical.

Work-piece:

MS strip: *25 mm* × *25 mm* × *8 mm* (thick)

Cu strip : *20 mm* × *20 mm* ×*10 mm* (thick)

Ti strip : *20 mm* × *20 mm* × *5 mm* (thick)

Graphite : *20 mm* × *20 mm* ×*10 mm* (thick)

Dielectric :

Kerosene : Breakdown voltage 23 V, Flash point 49 ^{0} C

ITW (company name): Mineral oil, low viscosity and odourless
Dielectric strength 45 kV and
Flash Point 93 ^{o} C

Discharge voltage : *40 V*

Input current : *20 amp,*

Pulse duration range used : 2-200 *μsec*

Flushing conditions: Side flushing with pressure 1.5 *bar*

Flushing flow rate: 1.5 *litre/min*

Time of machining: *15-20 min* (depending on the test)

For each pulse on-time, tests were repeated three times on fresh tool/work test pair and the average value of erosion rate estimated. *Weight loss method* was used for estimating the amount of material eroded during machining operation. The work-piece was mounted on the fixture and tool electrode was held in the collet. Initially the tool was brought down with the help of servo-motor by switching on the auto-positioning switch, so it would ensure the constant inter-electrode gap between tool and work-piece for particular voltage. Dielectric pump was switched on and once the level of dielectric reached above the safe limit, the low-level indicator goes off. Flushing valve was adjusted according to the requirement of the pressure.

The tests were performed for the pulse times varying from *2 μsec* upto *200 μsec*. At each of the pulse times used, the average current was noted down to an accuracy of 1 *amp*. After 15 - 20 *min* of machining, the weight of both the electrodes was measured with an electronic weighing machine and the amount of material eroded was measured. The erosion rates for an electrode was estimated by dividing the material eroded for that electrode by the duration of machining. The above procedure was repeated for eleven sets of electrode pairs, as shown in Table.2.1.

Nomenclature	Work (-ve) (Cathode)	Tool(+ve) (Anode)	Dielectric	Figure No.	Remarks
Case A	Gr	Gr	Kerosene	Fig 2.1,2.2,2.5,4.1,4.10	Similar Electrode Materials
Case B	Cu	Cu	ITW	Fig 2.2,2.3 ,2.5,4.3,4.11	
Case C	MS	MS		Fig 2.2,2.4,2.5,4.3,4.12	
Case D	MS	Cu		Fig 2.6,2.7,2.22,4.4,4.13	Dissimilar Electrode Material Pairs
Case E	Cu	MS		Fig 2.8,2.9,2.22	
Case F	Gr	Cu	Kerosene	2.10,2.11,2.22,4.6,4.14	
Case G	Cu	Gr		2.12,2.13,2.22,4.6,4.15	
Case H	Ti	Cu		2.14,2.15,2.23,4.7,4.16	
Case I	Cu	Ti		Fig 2.16,2.17,2.23	
Case J	Ti	MS		2.18,2.19,2.23,4.8,4.17	
Case K	MS	Ti		2.20,2.21,2.23,4.4,4.18	
Case B*	Cu	Cu	Kerosene	Fig C.1, C.4	Earlier work[36] on similar & Dissimilar material Pairs
Case C*	MS	MS		Fig C.2, C.4	
Case D*	MS	Cu		Fig C.3, C.5	
Case E*	Cu	MS		Fig C.5	

Table 2.1: Electrode pair combinations

The duty cycle position for all the experiments was kept constant at 10. A calibration chart supplied by the manufacturer (given in appendix A) gives the pulse off-time for different on-times for a particular value of duty cycle position. The amounts of material lost are presented in Tables 2.2 to 2.12.

2.3 Similar Tool and Work Material

Experimental observations of Cases B^*, C^*, D^* and E^* are those of by Saha [36]. And some experimental results are available in Appendix C.

2.3.1 Erosion Rates of Tool and work

Case A (*Gr / Gr* system):

Cathode (work) – Graphite

Anode (tool) - Graphite

Dielectric: Kerosene

The experimental observations for *Gr/Gr* system are presented in Table 2.2.

S.No.	Pulse On-time (μsec)	Pulse Off-time (μsec)	Average Current (*amps*)	Material Removal Rate		Work-tool Erosion ratio (WTER)
				Gr (-ve) (mm^3/min)	Gr (+ve) (mm^3/min)	
1	2	5	2	0.573	0.214	2.667
2	10	7	8	1.461	0.837	1.745
3	20	8	10	1.548	0.867	1.785
4	50	16	11	1.504	0.876	1.716
5	100	22	14	1.693	0.888	1.903
6	200	40	14	1.519	0.702	2.163

Table2.2: Experimental data for Case A: Cathode – Graphite; Anode – Graphite (Dielectric- Kerosene).

Variation of experimentally estimated cathode (Gr) and anode (Gr) erosion rates with pulse on-time is shown in Fig.2.1. Points in figure showing the experimental results. Based on these values a least mean square error fit is obtained using second order polynomial for the erosion rates of both cathode and anode against log of pulse on-time by using the software GNUPLOT (linux version 3.5). The erosion rate for cathode is obtained as

$$\dot{V}_{wc}\ (\text{Case A}) = 0.14429 + 0.7689 \ln(t_{on}) - 0.09752 (\ln(t_{on}))^2 \qquad \ldots(2.1)$$

And that for the anode is

$$\dot{V}_{wa}\ (\text{Case A}) = 0.1432 + 0.5891 \ln(t_{on}) - 0.0809 (\ln(t_{on}))^2 \qquad \ldots(2.2)$$

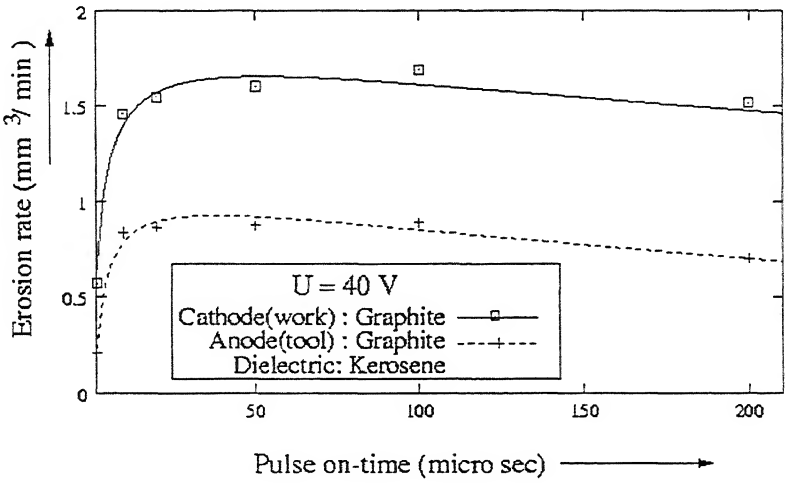

Fig. 2.1: Electrode erosion rate for Gr(-ve)/Gr(+ve) system (Dielectric: Kerosene)

Fig 2.1 shows the fact that the erosion rate of the cathode is greater than that of the anode. Erosion rate of both the electrodes first increases rapidly upto 50 μsec and then decreases slowly for longer pulse on-time. Conclusion from this figure is that the graphite work-piece should be connected to the cathode, for reduced tool wear.

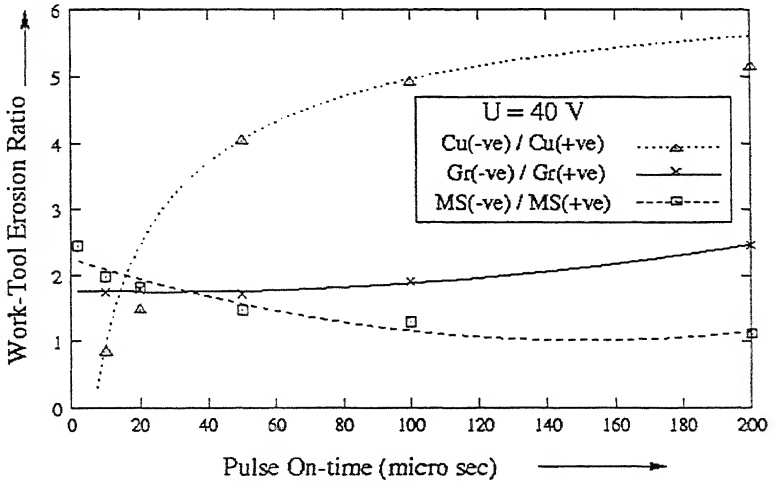

Fig. 2.2: Work-Tool Erosion Ratio for similar electrode material pair systems.

Work-Tool Erosion ratio (*Gr / Gr* system)

Work-Tool Erosion ratio (WTER) i.e., cathode erosion rate / anode erosion rate shown in Fig. 2.2 is obtained by fitting a second order polynomial for the experimental data points against pulse on-time. Figure shows that WTER remains nearly constant between 5 to 100 *μsec* pulse times and there after it increases. WTER should be maximum, for economical use of the EDM process. Hence, longer pulse on-time are recommended for machining operation when machining of graphite with graphite tool.

Case B (*Cu /Cu* system)

Cathode (work) - Copper

Anode (tool) – Copper

Dielectric: ITW

The experimental observations for *Cu/Cu* system are presented in Table 2.3.

S.No.	Pulse On-time (*μsec*)	Pulse Off-time (*μsec*)	Average Current (*amps*)	Material Removal Rate		Work-tool Erosion ratio (WTER)
				Cu (-ve) (mm^3/min)	Cu (+ve) (mm^3/min)	
1	2	5	2	0.254	0.1494	1.704
2	10	7	10	0.956	1.136	0.841
3	20	8	14	1.584	1.076	1.472
4	50	16	16	3.408	0.844	4.035
5	100	22	16	2.421	0.493	4.910
6	200	40	16	1.771	0.343	5.160

Table 2.3: Experimental data for Case B: Cathode(work) – Copper; Anode(tool) – Copper (dielectric - ITW)

Variation of experimentally estimated cathode (*Cu*) and anode (*Cu*) erosion rates with pulse on-time is shown in Fig 2.3. As before, a least mean square error fit is obtained for the erosion rates of both cathode and anode. The erosion rate for cathode is obtained as

$$\dot{V}_{wc}\ (\text{Case B}) = 0.14429 + 0.7689 \ln(t_{on}) - 0.09752 (\ln(t_{on}))^2 \qquad \ldots(2.3)$$

And that for the anode is

$$\dot{V}_{wa}\ (\text{Case B}) = 0.1432 + 0.5891 \ln(t_{on}) - 0.0809 (\ln(t_{on}))^2 \qquad \ldots(2.4)$$

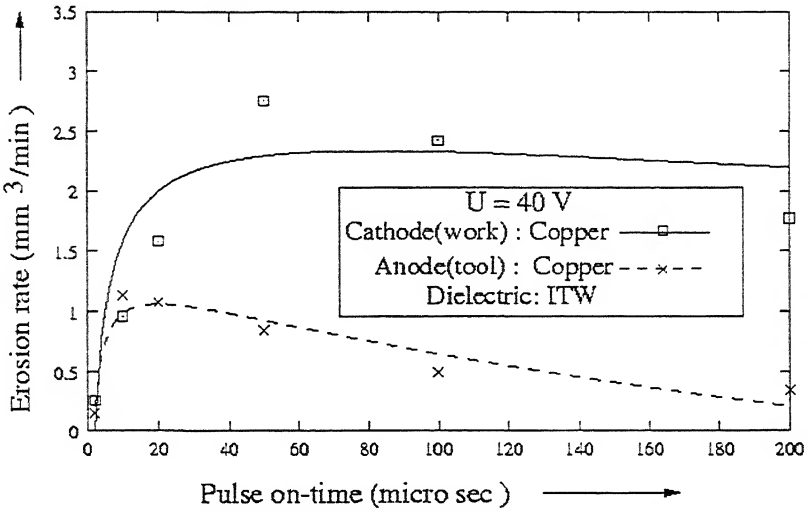

Fig. 2.3: Electrode erosion rate for Cu(-ve)/Cu(+ve) system (Dielectric: ITW).

Fig2.3 clearly shows that at very low pulse on-times (typically less than 5 *μsec*) only, the erosion rate of anode is more than that of the cathode. This indeed is the case of wire EDM operation. At all the other pulse on times the cathode (copper) erodes more than the anode (copper), which is usually the case of die-sinking operation in EDM process. This trend is agreement with the results of Heng et al. [15].

Work-Tool Erosion ratio (*Cu/Cu* system)

Variation of Work-Tool Erosion Ratio (WTER) with pulse on-time for this case is also shown in Fig. 2.2 is obtained as Case A. The figure shows that WTER increases first then remains nearly constant (between 100 to 200 *μsec*) pulse times for a wide range of pulse on-time. Therefore for economical used of the process, one will have wide range of choice of pulse time when both electrodes are of copper. *The value of WTER is 5 for longer on-time which is quantitatively in agreement with the experimental results of Longfellow et al. [25] (WTER reported by Longfellow is 4.8 for Cu/Cu case).* WTER should be maximum, for economical use of the EDM

process. Hence, longer pulse on-time are recommended for machining of copper with copper tool.

Case C (*MS /MS* system)

Cathode (work) – Mild-Steel

Anode (tool) – Mild-Steel

Dielectric: ITW

The experimental observations for *MS/MS* system are presented in Table2.4.

S.No.	Pulse On-time (μsec)	Pulse Off-time (μsec)	Average Current (*amps*)	Material Removal Rate		Work-tool Erosion ratio (WTER)
				MS (-ve) (mm^3/min)	MS(+ve) (mm^3/min)	
1	2	5	3	0.164	0.067	2.447
2	10	7	13	1.624	0.821	1.976
3	20	8	15	1.537	0.848	1.812
4	50	16	15	1.113	0.759	1.466
5	100	22	15	0.901	0.698	1.291
6	200	40	15	0.663	0.592	1.119

Table2.4: Experimental data for Case C : Cathode (work)– Mild-Steel; Anode(tool) – Mild-Steel. Dielectric - ITW

Fig 2.5 shows the variation of experimentally estimated cathode (*MS*) and anode (*MS*) erosion rates with pulse on-time. As before, a least mean square error fit is obtained for the erosion rates of both cathode and anode. The erosion rate for cathode is obtained as

$$\dot{V}_{wc}\ (\text{Case C}) = -0.5539 + 1.319 \ln(t_{on}) - 0.2119(\ln(t_{on}))^2 \qquad \ldots(2.5)$$

And that for the anode is

$$(\text{Case C}) = -0.3284 + 0.6862 \ln(t_{on}) - 0.0987 (\ln(t_{on}))^2 \qquad \ldots(2.6)$$

This figure also depicts the facts that the erosion rate of cathode is greater than that of anode. It appears that the maximum erosion rate of both the electrodes occurs in the same range of pulse on-time, i.e., 20 to 40 *μsec*. Beyond a certain pulse on-time (typically 40 *μsec*), the erosion rate of cathode decreases drastically while that of anode remains more or less constant.

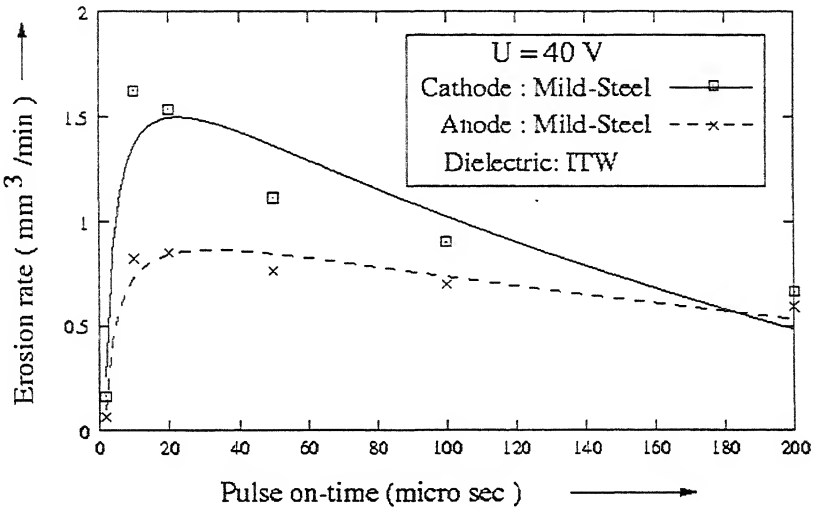

Fig. 2.4: Electrode erosion rate for MS(-ve)/MS(+ve) system(Dielectric: ITW)

Work-Tool Erosion ratio (*MS/MS* system)

Variation of Work-Tool Erosion ratio (WTER) with pulse on-time shown in Fig. 2.2 is obtained as Case A. This figure shows that WTER decreases slowly from low pulse on times. In practical range of operation i.e., maximum WTER (at low pulse on times) which is about 2.4 is quantitatively in agreement with the results of Longfellow et al. [25] (WTER reported by longfellow is 2.5 for MS/MS case). For economical use of the process, low pulse on-time are recommended for machining of mild-steel with mild-steel tool.

2.3.2 Average current *Vs* Pulse On-time

The variation of average current with pulse On-time observed in similar electrode material pair i.e. Case A, B & C is shown in Fig.2.5. In these experiments, the current

passing though the gap during machining process was found to rise and stabilizes in accordance with the following relation of type

$$I = a - b \times e^{\left(-t_{on}/c\right)}$$

and values of *a, b, c* were obtained using the software GNUPLOT (Linux version 3.5).

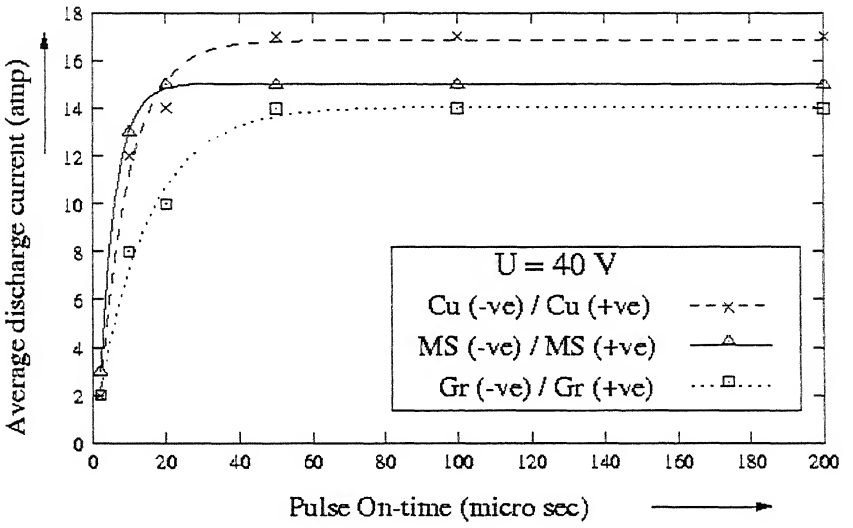

Fig. 2.5 a: Average discharge current for similar electrode pair systems.

And the relation between (I) and (t_{on}) for each case is obtained as.

For (Case A) $I = 13.205 - 12.51e^{\left(-t_{on}/13.877\right)}$ ...(2.7)

(Case B) $I = 16.871 - 17.124e^{\left(-t_{on}/8.972\right)}$ ...(2.8)

and (Case C) $I = 15.044 - 18.865e^{\left(-t_{on}/4.459\right)}$ ...(2.9)

Where t_{on} is measured in μsec and I in amp.

2.3.3 Interim conclusions (similar tool and work material)

On the basis of experimental observation presented in Figs 2.1, 2.2, 2.3, 2.4 and 2.5 following conclusions can be derived.

1. Cathode erosion rate is higher than anode erosion rate for the range of pulse on-time utilized. Hence for high WTER, work should be connected to cathode in EDM die-sinking operation.
2. Erosion rate of Copper is highest followed by Mild-Steel and than by Graphite.
3. There is an optimum pulse on-time at which the erosion rate of cathode (work) is highest.
4. There is an increasing trend of WTER except in MS/MS system, where it is decreasing. For economical machining, WTER should be maximum. So choice of the range of pulse on-time for machining operation varies with the different electrode system.
5. *Specific heat* is the only thermo-physical property, which is showing some trend with average discharge current for similar material electrode pair as shown in Fig.2.5 b. Since average current results due to the flow of electrons changes with change in electrode material. Upto 20 μsec, the resistance to the flow of electrons appears to follow the order as show below as shown in Fig2.5 a.

   Case C > Case B > Case A

   However, beyond about 20 μsec, the order of resistance to the flow of electrons is

   Case B > Case C > Case A

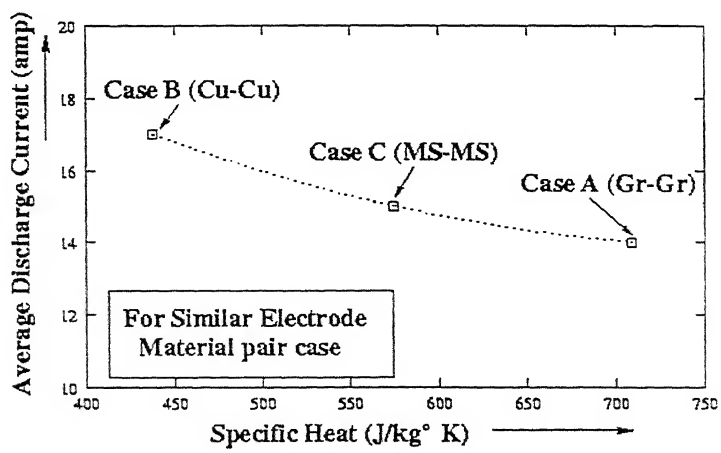

Fig. 2.5 b: Average discharge current with specific heat for similar electrode pair

2.4 Dissimilar Tool and Work material

2.4.1 Erosion rates of tool and work

Case D (*MS /Cu* system)

Cathode (work) – Mild-Steel

Anode (tool) – Copper

Dielectric: ITW

The experimental observations for *MS/Cu* system are presented in Table 2.5.

S.No.	Pulse On-time (μsec)	Pulse Off-time (μsec)	Average Current (*amps*)	Material Removal Rate		Work-tool Erosion ratio (WTER)
				MS (-ve) (mm^3/min)	Cu (+ve) (mm^3/min)	
1	2	5	3	0.106	0.145	0.727
2	5	7	7	3.962	6.647	0.596
3	10	7	9	21.510	7.937	2.710
4	20	8	12	26.600	6.647	4.001
5	100	22	15	13.783	1.773	7.785
6	200	40	15	12.776	0.9608	12.276

Table 2.5: Experimental data for Case D: Cathode (work) – Mild-Steel; Anode(tool) – Copper; Dielectric- ITW

Fig 2.6 depicts the variation of experimentally estimated cathode (*MS*) and anode (*Cu*) erosion rates with pulse on-time. As before, a least mean square error fit is obtained for the erosion rates of both cathode and anode. The erosion rate for cathode is obtained as

$$\dot{V}_{wc}\ (\text{Case D}) = -17.095 + 23.332 \ln(t_{on}) - 3.408 (\ln(t_{on}))^2 \quad \ldots(2.10)$$

And that for the anode is

$$\dot{V}_{wa}\ (\text{Case D}) = -3.481 + 7.685 \ln(t_{on}) - 1.367 (\ln(t_{on}))^2 \quad \ldots(2.11)$$

From Fig 2.6 it is evident that *the erosion rate of cathode (MS) is always more than that of the anode (Cu).* This is qualitatively in conformity with the results of DiBitonto et al.[5] and Snoeys et al. [39] for die-steel.

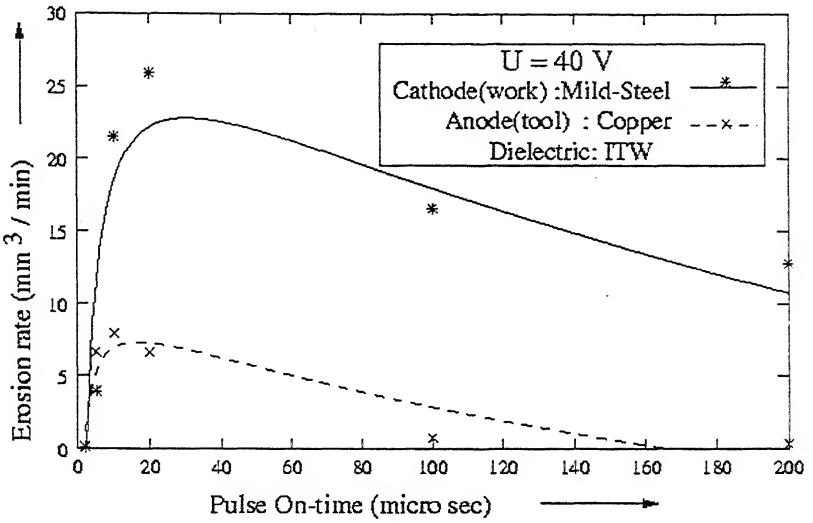

Fig. 2.6: Electrode erosion rate for MS(-ve)/Cu(+ve) system.

Work-Tool erosion rate (*MS/Cu* system)

The variation of WTER with pulse on-time is obtained as in Case A and shown in Fig.2.7. From this figure it is clear that the WTER increases with pulse time. This qualitatively agrees with the results of George et al. [12] for die-steel. This means that to maximize the erosion rate of work-piece, the work-piece (Mild-Steel) should be connected to cathode. This indeed is the case with usual die-sinking operation.

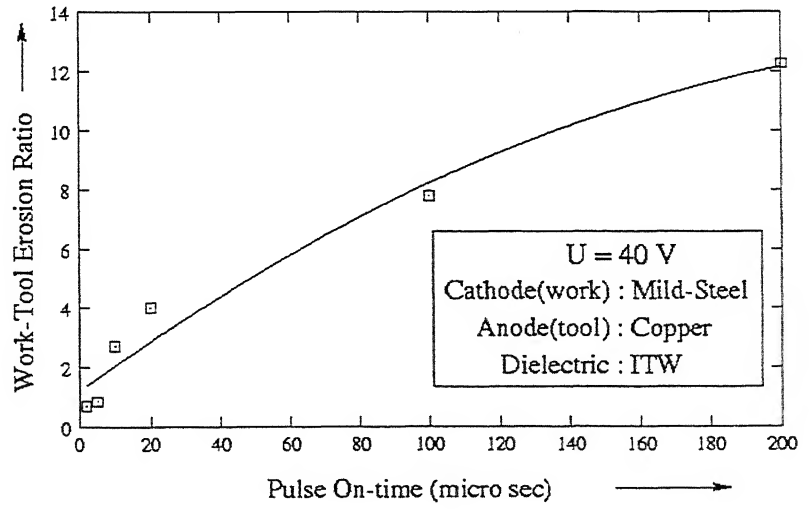

Fig. 2.7: Work-Tool Erosion Ratio for MS(-ve)/Cu(+ve) system

Case E (*Cu / MS* system)

Cathode (work)– Copper

Anode (tool)– Mild-steel

Dielectric: ITW

The experimental observations for *Cu/MS* system are presented in Table 2.6.

S.No.	Pulse On-time (*μsec*)	Pulse Off-time (*μsec*)	Average Current (*amps*)	Material Removal Rate		Work-tool Erosion ratio (WTER)
				Cu (-ve) (mm^3/min)	MS (+ve) (mm^3/min)	
1	2	5	3	0.067	0.357	0.1878
2	5	7	6	0.408	1.179	0.3459
3	10	7	7	0.179	0.429	0.4157
4	20	8	10	0.049	0.161	0.305
5	100	22	13	0.007	0.180	0.0404
6	200	40	13	0.007	0.149	0.0487

Table 2.6: Experimental data for Case E: Cathode(work) – Copper; Anode(tool) – Mild-Steel (Dielectric: ITW)

Fig 2.8 depicts the variation of experimentally estimated cathode (*Cu*) and anode (*MS*) erosion rates with pulse on-time. Beyond 20 *μsec* pulse time, the erosion rates of the electrodes were very low. The least mean square fit in this case could not be obtained. This trends agree with the result of earlier work [36] on kerosene dielectric. Trend is also in conformity with the results of Albinki [1]. Fig 2.8 it is clearly seen that, contradictory to the other cases as shown in Case A, B, C and D, *the erosion rate of anode (Mild-Steel) is more than that of the cathode (copper).* The values of erosion rates from the electrodes is changed with changing the dielectric and other parameters of machining, but the general trend is expected to the same as in Fig 2.8.

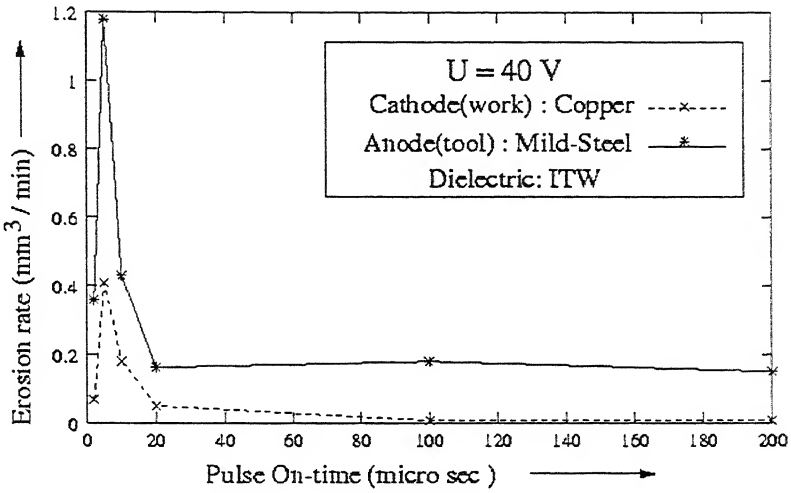

Fig. 2.8: Electrode erosion rate for Cu(-ve)/MS(+ve) system

In this case the WTER decreases with increase with pulse on-time as shown in Fig 2.9. However its values are low (less than 1). Since WTER is less than 1, this system is not recommended for practical machining.

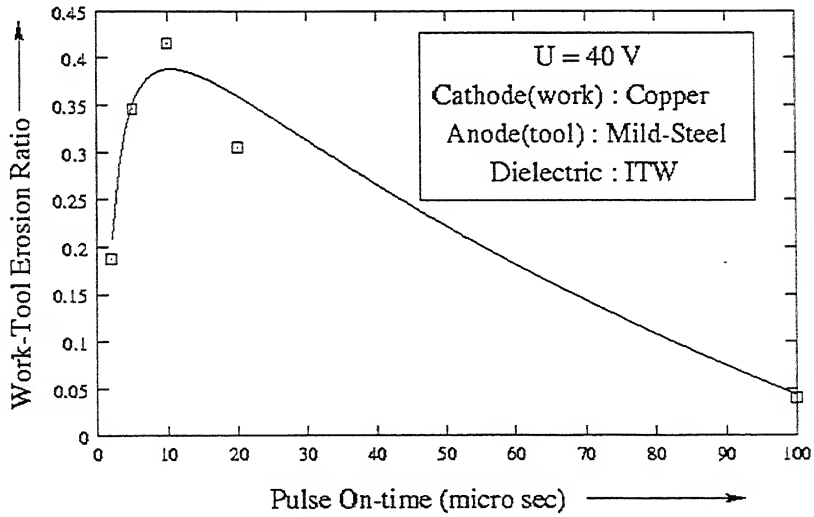

Fig. 2.9: Work-Tool Erosion Ratio for Cu(-ve)/MS(+ve) system.

Case F (*Gr/Cu* system)

Cathode (work) – Graphite

Anode (tool)– Copper

Dielectric: ITW

The experimental observations for Gr/Cu system are presented in Table 2.7.

S.No.	Pulse On-time (μsec)	Pulse Off-time (μsec)	Average Current (*amps*)	Material Removal Rate		Work-tool Erosion ratio (WTER)
				Gr (-ve) (mm^3/min)	Cu (+ve) (mm^3/min)	
1	2	5	2	1.161	0.560	2.072
2	10	7	5	1.203	0.834	1.442
3	20	8	10	2.206	0.988	2.231
4	50	16	10	2.709	1.049	2.582
5	100	22	13	3.282	1.136	2.889
6	200	40	14	3.081	0.861	3.578

Table 2.7: Experimental data for Case F: Cathode – Graphite; Anode – Copper (Dielectric: ITW).

Fig 2.10 depicts the variation of experimentally estimated cathode (*Gr*) and anode (*Cu*) erosion rates with pulse on-time. As before, a least mean square error fit is obtained for the erosion rates of both cathode and anode.

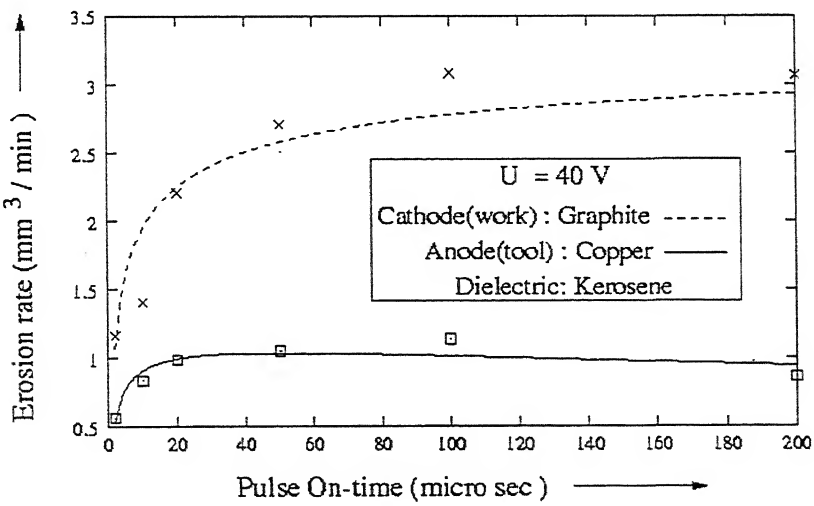

Fig. 2.10: Electrode erosion rate for Gr(-ve)/Cu(+ve) system.

Trend is similar to the earlier cases. The erosion rate for cathode is obtained as

$$\dot{V}_{wc} \text{ (Case E)} = 0.615 + 0.378 \ln(t_{on}) - 0.0482 (\ln(t_{on}))^2 \qquad \ldots(2.12)$$

And that for the anode is

$$\dot{V}_{wa}\ (\text{Case E}) = 0.292 + 0.683\ln(t_{on}) - 0.0462\,(\ln(t_{on}))^2 \qquad \ldots(2.13)$$

The variation of WTER with pulse on time is shown in Fig 2.11. And the trend is similar to Case D (MS(-ve)/Cu(+ve) system) of Fig 2.7. In Case D, Copper is also used as anode.

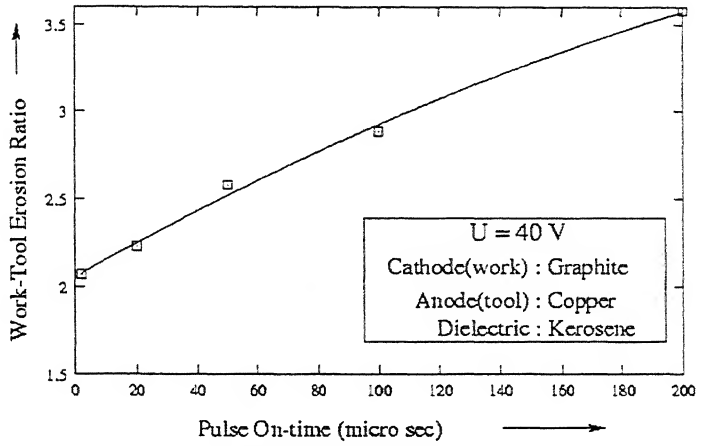

Fig. 2.11: Work-Tool Erosion Ratio for Gr(-ve)/Cu(+ve) system.

Case G (*Cu/Gr* system)

Cathode (work) – Copper

Anode (tool) – Graphite

Dielectric: Kerosene

The experimental observation for *Cu/Gr* system is presented in Table 2.8.

S.No.	Pulse On-time (μsec)	Pulse Off-time (μsec)	Average Current (*amps*)	Material Removal Rate		Work-tool Erosion ratio (WTER)
				Cu (-ve) (mm^3/min)	Gr (+ve) (mm^3/min)	
1	2	5	3	0.102	0.573	0.178
2	10	7	7	0.428	1.002	0.427
3	20	8	10	0.867	1.226	0.707
4	50	16	11	1.188	1.318	0.901
5	100	22	12	1.103	1.135	0.971
6	200	40	12	0.841	1.097	0.766

Table 2.8: Experimental data for Case G: Cathode – Copper; Anode – Graphite.

Fig.2.12. depicts the variation of the estimated cathode (*Cu*) and anode (*Gr*) erosion rates with pulse on-time. As before, a least mean square error fit is obtained for the erosion rates of both cathode and anode. The erosion rate for cathode is obtained as

$$\dot{V}_{wc} \text{ (Case G)} = -0.370 + 0.610 \ln (t_{on}) - 0.067 (\ln(t_{on}))^2 \qquad \ldots(2.14)$$

And that for the anode is

$$\dot{V}_{wa} \text{ (Case G)} = 0.219 + 0.533 \ln (t_{on}) - 0.0696 (\ln(t_{on}))^2 \qquad \ldots(2.15)$$

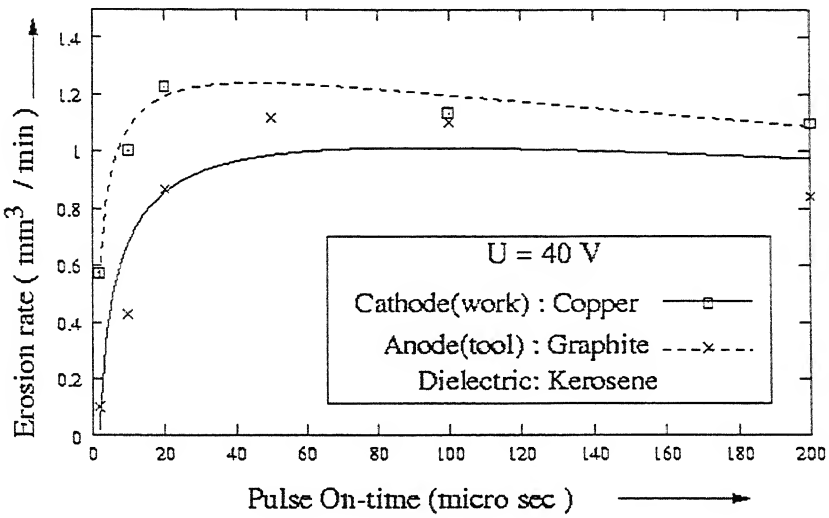

Fig. 2.12: Electrode erosion rate for Cu(-ve)/Gr(+ve) system.

Fig 2.13 shows the variation of WTER with pulse on-time for this case, and values of WTER are less than 1. Erosion rate of anode (Graphite) is more which is similar to Case E (*Cu(-ve)/MS*(+ve)system).

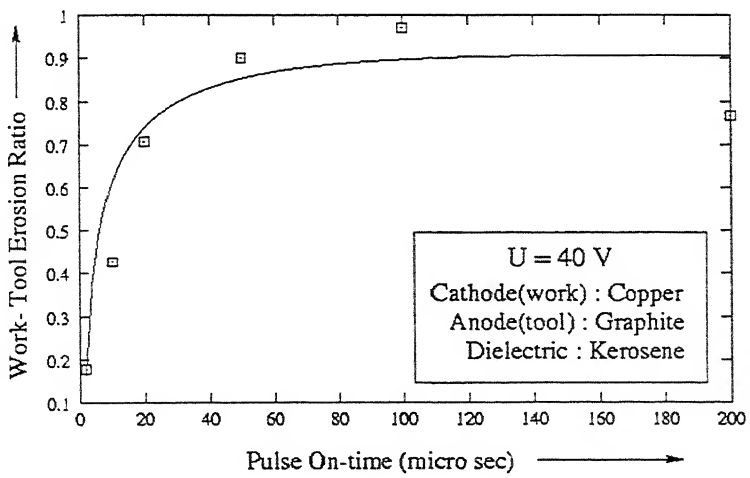

Fig. 2.13: Work-Tool Erosion Ratio for Cu(-ve)/Gr(+ve) system.

Case H (*Ti/Cu* system)

Cathode (work) – Titanium

Anode (tool)– Copper

Dielectric: Kerosene

The experimental observation for Ti/Cu system is presented in Table 2.9.

S.No.	Pulse On-time (μsec)	Pulse Off-time (μsec)	Average Current (*amps*)	Material Removal Rate		Work-tool Erosion ratio (WTER)
				Ti (-ve) (mm^3/min)	Cu (+ve) (mm^3/min)	
1	2	5	2	0.123	0.155	0.797
2	5	7	5	0.583	0.727	0.801
3	10	7	9	0.874	0.755	1.628
4	20	8	10	1.022	0.392	1.415
5	50	16	12	1.072	0.272	3.946
6	100	22	12	1.141	0.262	5.305
7	200	40	12	1.066	0.157	6.798

Table 2.9: Experimental data for Case H: Cathode – Titanium; Anode – Copper.

Fig 2.16 depicts the variation of experimentally estimated cathode (*Ti*) and anode (*Cu*) erosion rates with pulse on-time. As before, a least mean square error fit is obtained for the erosion rates of both cathode and anode.

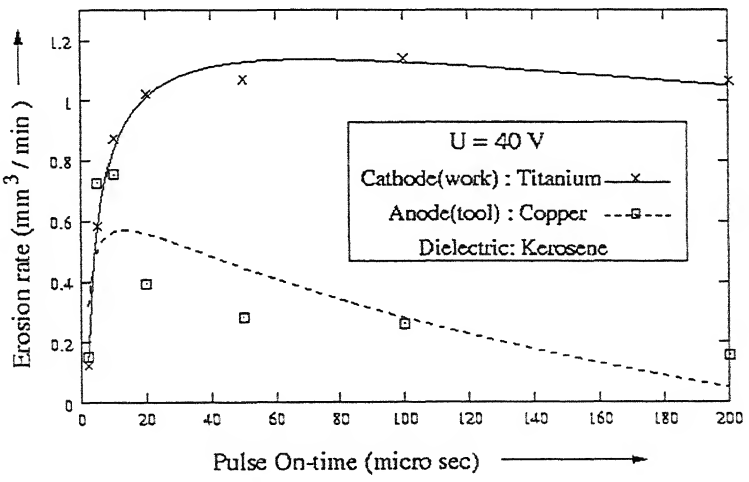

Fig. 2.14: Electrode erosion rate for Ti(-ve)/Cu(+ve) system.

The erosion rate for cathode is obtained as

$$\dot{V}_{wc} \text{ (Case H)} = 0.104 + 0.361 \ln (t_{on}) - 0.070 (\ln(t_{on}))^2 \quad \ldots(2.16)$$

And that for the anode is

$$\dot{V}_{wa} \text{ (Case H)} = -0.292 + 0.671 \ln (t_{on}) - 0.078 (\ln(t_{on}))^2 \quad \ldots(2.17)$$

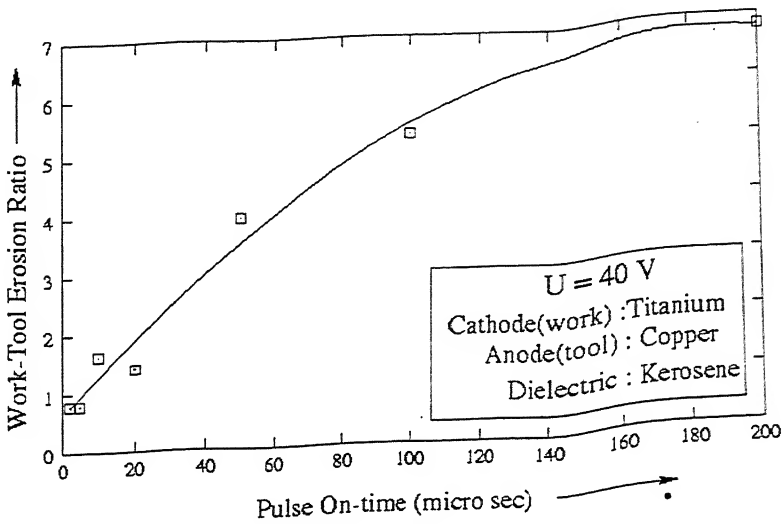

Fig. 2.15: Work-Tool Erosion Ratio for Ti(-ve)/Cu(+ve) system.

Fig 2.14 shows similar results to that of the Case D and F i.e. copper is connected to positive polarity. The erosion rates of cathode are more than anode when copper is used as an anode. And also the variation of WTER with pulse on-time is shown in Fig 2.15, having the trend similar to the Case D and F.

Case I (*Cu/Ti* system)

Cathode (work) – Copper

Anode (tool) – Titanium

Dielectric: Kerosene

The experimental observations for Cu/Ti system are presented in Table 2.10. Fig 2.16 depicts the variation of experimentally estimated cathode (*Cu*) and anode (*Ti*) erosion rates with pulse on-time.

S.No.	Pulse On-time (μsec)	Pulse Off-time (μsec)	Average Current (*amps*)	Material Removal Rate		Work-tool Erosion ratio (WTER)
				Cu (-ve) (mm^3/min)	Ti (+ve) (mm^3/min)	
1	2	5	2	0.037	0.093	0.399
2	5	7	4	0.451	0.562	0.802
3	10	7	8	0.693	1.322	0.524
4	20	8	10	0.491	0.884	0.555
5	50	16	11	0.045	0.410	0.109
6	100	22	11	0.035	0.375	0.094
7	200	40	11	0.032	0.336	0.095

Table 2.10: Experimental data for Case I: Cathode(work) – Copper; Anode(tool) – Titanium.

Trend of electrode erosion rates are quite similar to that of Case E (Cu(-ve)/Ms(+ve) system). Like this case, copper was made cathode in Case E also. Electrode erosion rates are very low beyond 50μsec, so least square fitting could not be obtained in this case also.

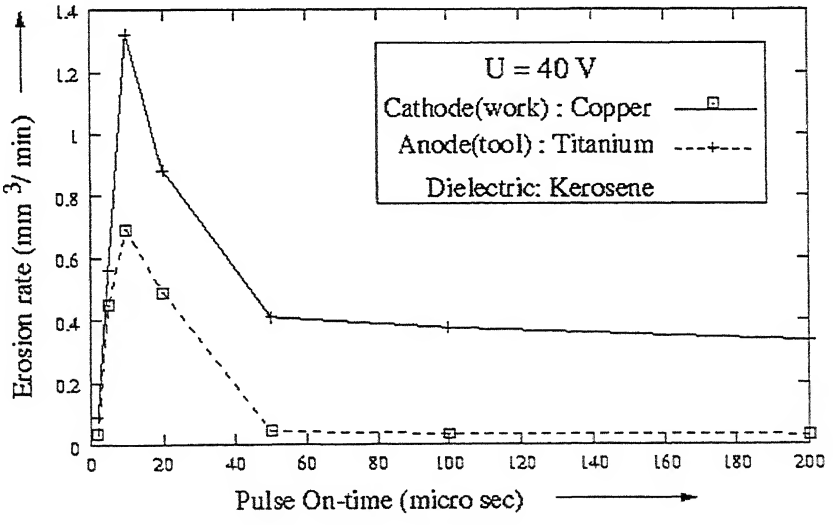

Fig. 2.16: Electrode erosion rate for Cu(-ve)/Ti(+ve) system.

The variation of WTER with pulse time is showing the same trend to that of Case E and G i.e. copper is connected to negative polarity and value is less than 1 as shown in Fig 2.17. So it is concluded that erosion rate of Titanium is more than copper in any case either it is connected to cathode or anode with copper.

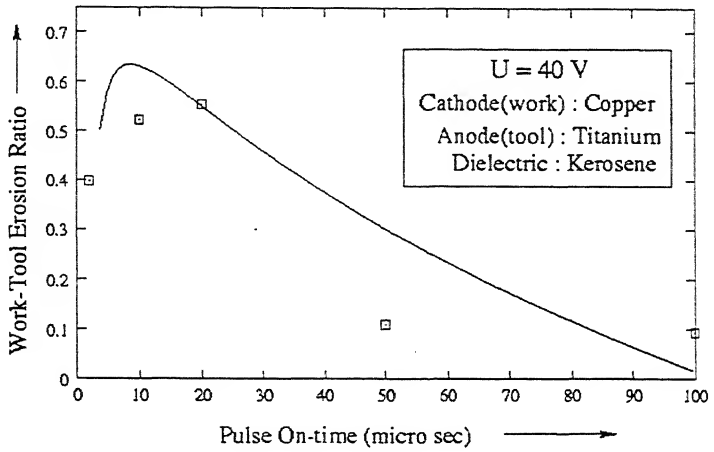

Fig. 2.17: Work-Tool Erosion Ratio for Cu(-ve)/Ti(+ve) system.

Case J (*Ti/MS* system)

Cathode (work)– Titanium

Anode (tool)– Mild-steel

Dielectric: kerosene

The experimental observations for Ti/MS system are presented in Table 2.11.

S.No.	Pulse On-time (μsec)	Pulse Off-time (μsec)	Average Current (*amps*)	Material Removal Rate		Work-tool Erosion ratio (WTER)
				Ti (-ve) (mm^3/min)	MS (+ve) (mm^3/min)	
1	2	5	2	0.064	0.029	2.180
2	5	7	8	0.153	0.185	0.825
3	10	7	12	0.133	0.262	0.508
4	20	8	12	0.104	0.242	0.429
5	50	16	12	0.079	0.227	0.348
6	100	22	12	0.054	0.215	0.253
7	200	40	12	0.054	0.118	0.461

Table 2.11: Experimental data for Case J: Cathode – Titanium; Anode –Mild Steel.

Fig 2.20 shows the variation of experimentally estimated cathode (Ti) and anode (MS) erosion rates with pulse on-time. As before, a least mean square error fit is obtained for the erosion rates of both cathode and anode. Trend is similar to the earlier results. The erosion rate for cathode is obtained as

$$\dot{V}_{wc} \text{ (Case J)} = 0.058 + 0.051 \ln (t_{on}) - 0.0104 (\ln(t_{on}))^2 \qquad \ldots(2.18)$$

And that for the anode is

$$\dot{V}_{wa} \text{ (Case J)} = -0.097 + 0.224 \ln (t_{on}) - 0.0346 (\ln(t_{on}))^2 \qquad \ldots(2.19)$$

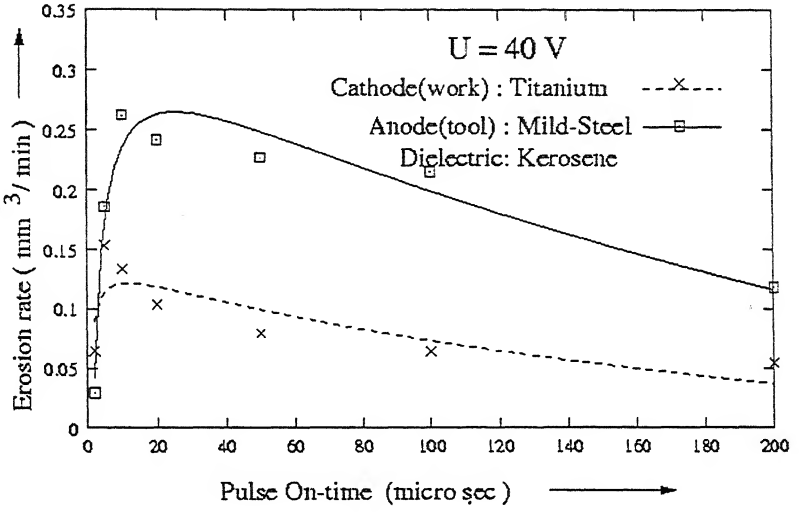

Fig. 2.18: Electrode erosion rate for Ti(-ve)/MS(+ve) system.

Fig 2.19 shows the variation of WTER with pulse on-time. And its values are less than 1. This concludes that the erosion rates of mild-steel are more than titanium.

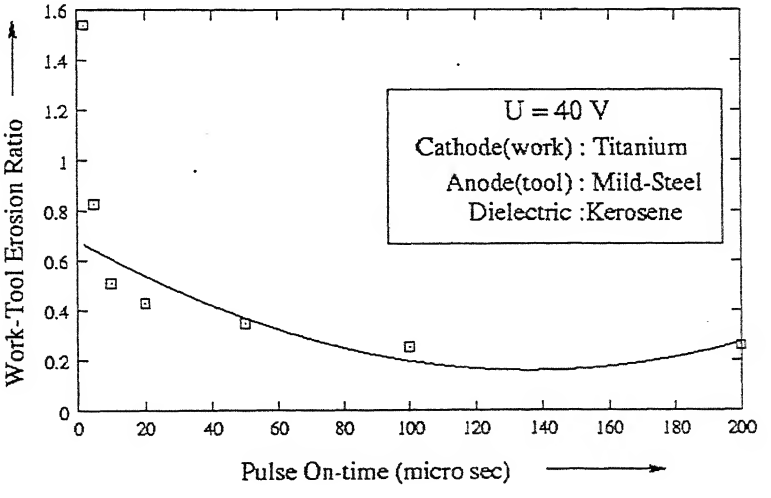

Fig. 2.19: Work-Tool Erosion Ratio for Ti(-ve)/MS(+ve) system.

Case K (*MS/Ti* system)

Cathode (work) – Mild-Steel

Anode (tool) – Titanium

Dielectric: kerosene

The experimental observations for MS/Ti system are presented in Table 2.12. Fig 2.7 shows the variation of experimentally estimated cathode (*MS*) and anode (*Ti*) erosion rates with pulse on-time. As before, a least mean square error fit is obtained for the erosion rates of both cathode and anode.

S.No.	Pulse On-time (μsec)	Pulse Off-time (μsec)	Average Current (*amps*)	Material Removal Rate		Work-tool Erosion ratio (WTER)
				MS (-ve) (mm^3/min)	Ti (+ve) (mm^3/min)	
1	2	5	2	0.318	0.094	3.394
2	5	7	8	1.384	0.163	8.499
3	10	7	12	1.749	0.183	9.581
4	20	8	12	2.147	0.188	11.451
5	50	16	12	3.025	0.232	13.036
6	100	22	12	3.333	0.242	13.791
7	200	40	12	3.145	0.197	15.940

Table 2.12: Experimental data for Case K: Cathode – Mild Steel; Anode – Titanium.

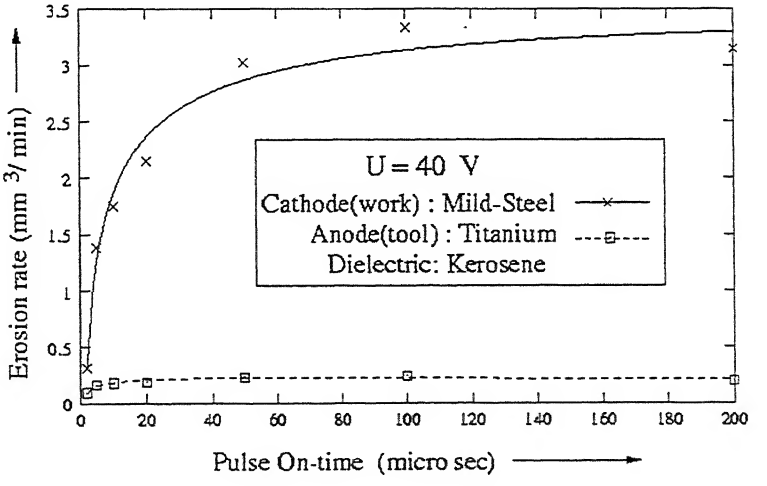

Fig. 2.20: Electrode erosion rate for MS(-ve)/Ti(+ve) system

The erosion rate for cathode is obtained as

$$\dot{V}_{wc} \text{ (Case K)} = -0.514 + 1.269 \ln (t_{on}) - 0.103 (\ln(t_{on}))^2 \qquad \ldots(2.20)$$

And that for the anode is

$$\dot{V}_{wa} \text{ (Case K)} = 0.0383 + 0.0883 \ln (t_{on}) - 0.0105 (\ln(t_{on}))^2 \qquad \ldots(2.21)$$

The variation of WTER with pulse on-time is shown in Fig 2.21. WTER value increases first then nearly constant for higher pulse time. There is wide choice of pulse time for machining in this case. Erosion of cathode (mild-steel) is nearly 15 times more than anode (Titanium). It has similar trend to that of Case B. So from above two Cases J and K it is concluded that erosion rate of Mild-steel is more than Titanium in any case either it is connected to cathode or anode.

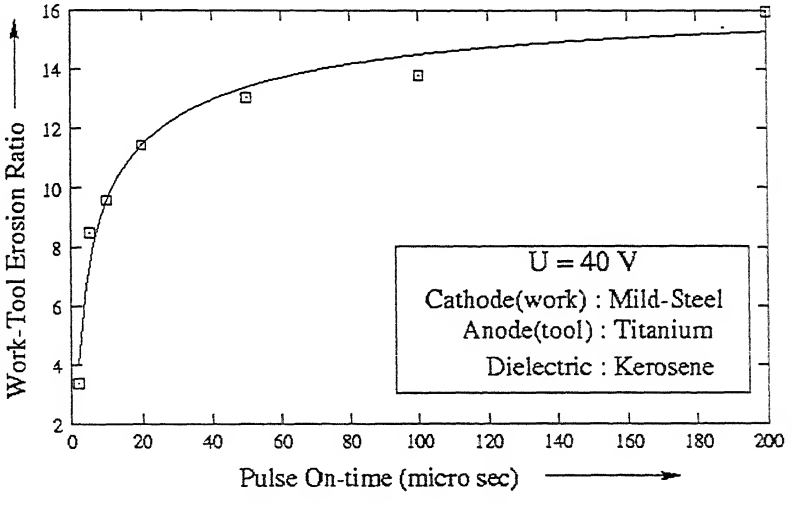

Fig. 2.21: Work-Tool Erosion Ratio for MS(-ve)/Ti(+ve) system.

2.4.2 Average current *Vs* Pulse On-time

Fig.2.15 shows the variation of the average current (I) with on-time (t_{on}) obtained as in *Sec 2.3.2*, for electrode pair of dissimilar materials case i.e., for Case D, E, F, G, H, I, J and K.

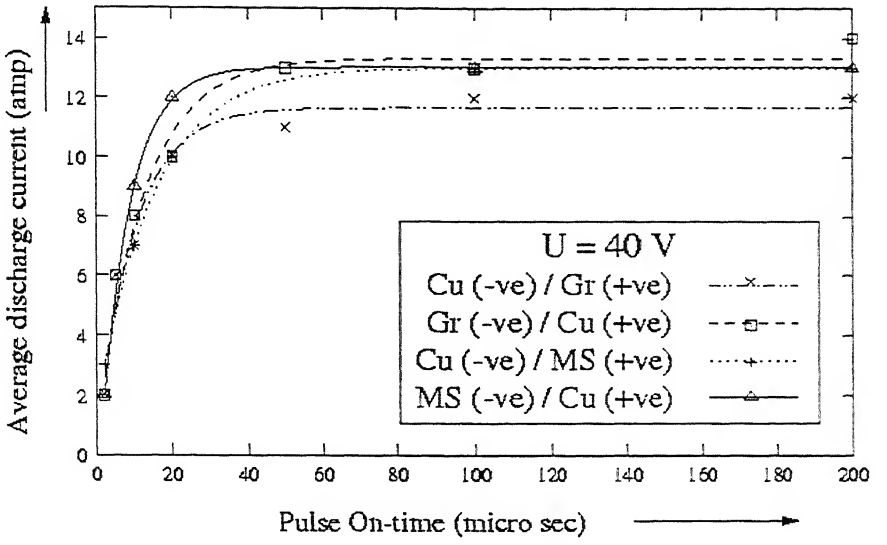

Fig. 2.22: Average discharge current for dissimilar electrode pair systems.

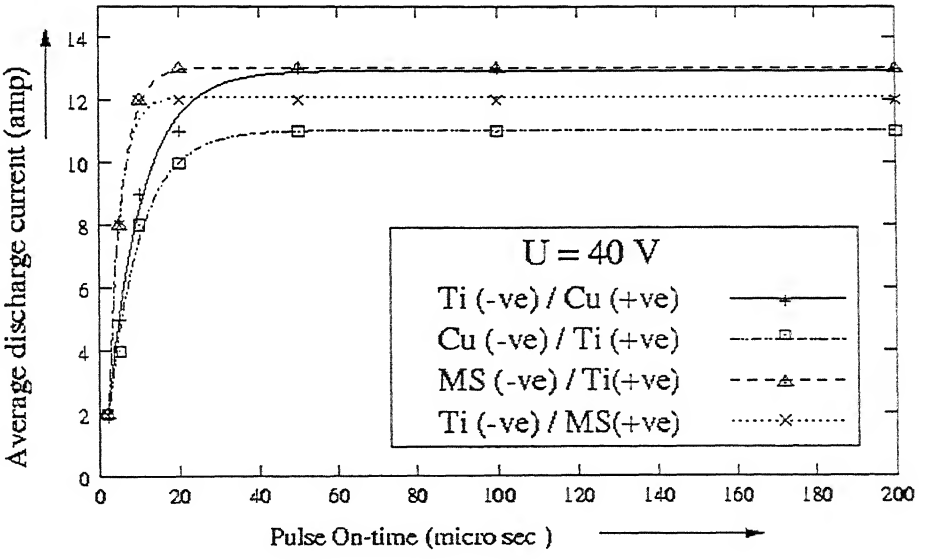

Fig. 2.23: Average discharge current for dissimilar electrode pair systems.

And the relation between (I) and (t_{on}) for each case is given as.

For (Case D) $I = 13.021 - 14.244e^{\left(-t_{on}/7.824\right)}$ ...(2.22)

(Case E) $I = 13.015 - 11.448e^{\left(-t_{on}/15.235\right)}$ ...(2.23)

(Case F) $I = 13.325 - 12.401e^{\left(-t_{on}/112.577\right)}$ ...(2.24)

(Case G) $I = 11.665 - 11.071e^{\left(-t_{on}/10.105\right)}$ ...(2.25)

(Case H) $I = 12.944 - 13.711e^{\left(-t_{on}/8.83\right)}$ ...(2.26)

(Case I) $I = 11.031 - 11.888e^{\left(-t_{on}/8.116\right)}$ ...(2.27)

(Case J) $I = 12.102 - 19.678e^{\left(-t_{on}/3.032\right)}$ ...(2.28)

and (Case K) $I = 13.046 - 19.110e^{\left(-t_{on}/3.673\right)}$ ...(2.29)

Where t_{on} is measured in μsec and I in amp

2.4.3 Interim conclusion (dissimilar tool and work material)

On the basis of experimental observation presented in Figs 2.5 to 2.23 following conclusions can be derived.

Erosion rate of cathode is not necessarily always higher than that of anode. The erosion rate depends on the material of the other electrode. A single thermo-physical property can not be associated with the trend shown by Table 2.13. However on the basis thermo-physical properties Table 3.1, following interference may be drawn.

1. The electrode material having lower thermal conductivity K_T in comparison to other electrode erodes more. Table 2.13 also shows the same trend except for Ti/MS case i.e. Case J and K. In this case the difference in thermal conductivity is not much significant and other material characteristics may be dominating over thermal conductivity which shows the exceptional behaviour.
2. Pandey [30] stated that deeper and wider craters are associated with the material having low erosion strength (defined as $K_T \rho C T_m^2$) and hence high erosion strength is desired for the tool material. This observation is also verified in the present study with the exception of Ti/MS case. This shows that the effects of different material properties are required to be studied in exceptional cases.

Work (cathode)	Tool (anode)	WTER (cathode/anode)
Mild-Steel	Copper	>>1
	Titanium	>1
Graphite	Copper	>>1
Titanium	Copper	>>1
	Mild-Steel	<1
Copper	Mid-Steel	<1
	Graphite	<1
	Titanium	<1

Table 2.13: Trend of WTER for different cases

3. Similar trend of electrode erosion rate and WTER can be seen in the Case E and I i.e., when Cu is used as cathode with MS and Ti anode respectively. In both the case erosion rate is very low beyond the 20 $\mu sec.$

Chapter 3

THEORETICAL ESTIMATES

The present study, extends an earlier work [36] for *cathode* erosion using *Pointed Heat Source Model* (PHSM) [5] for some more combination of tool and work materials shown in Table 2.1. An attempt has also been made to compare the experimentally estimated *anode* erosion rates with the theoretical estimates based on *Expanding Circular Heat Source Model* (ECHSM) [34]. Generally, thermal models are considered equally applicable to cathode or anode and hence do not explain inequal erosion rates for an identical cathode and anode material pair. Dibitonto et al. [5] and Patel et al. [34] however, explained that erosion of cathode should be based on the PHSM whereas the erosion of anode should be explicable on the basis of ECHSM. Following sections explain these fully.

3.1 Theoretical Estimates of Cathode

Cathode erosion estimates is based on PHSM developed by DiBitonto et al. [5] and is discussed below.

3.1.1 Pointed Heat source Model.

The main assumptions of the model are following.

1. There is only one spark per pulse and the plasma radius is very small ($< 5\ \mu m$)
   - *This is strictly true for only single grain material.*
2. Effective (average) thermo-physical properties of the cathodic material apply over the temperature range from solid to liquid melt.
   - *This is obviously to simplify calculations.*
3. A constant fraction f_c of the total power (UI) is lost to the cathode, independent of the current and pulse time. This fraction may change from different dielectric or electrode materials.
   - *No proof is available for its validity.*

Fig 3.1 illustrates the spherical symmetry resulting from the above assumptions as well as the melt front radius *R(t)*.

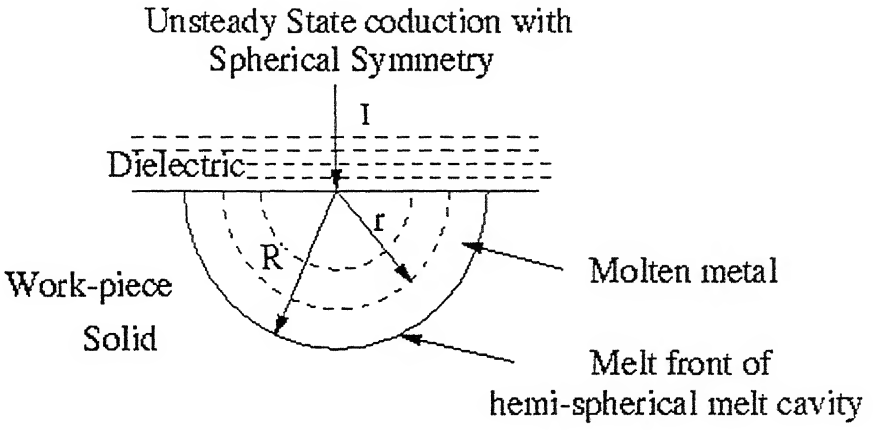

Fig 3.1 Cathode erosion of pointed heat source model.

- *This would be true for homogeneous single-phase material.*

The governing partial differential equation for this heat conduction problem without heat generation is

$$\frac{1}{\alpha}\frac{\partial T}{\partial t} = \frac{\partial^2 T}{\partial r^2} + \frac{2}{r}\frac{\partial T}{\partial r} \qquad \ldots(3.1)$$

And associated initial and boundary conditions as:

$$\begin{aligned} &IC: t = 0, \text{ for all } r,\ T = T_o, \\ &BC: t > 0, -K_T \frac{\partial T}{\partial r} = q_o \quad \text{for } r = 0 \\ &\qquad -K_T \frac{\partial T}{\partial r} = 0, \quad \text{for } r \neq 0 \\ &BC: t > 0, \quad r = \infty, \quad T = T_o, \end{aligned} \qquad \ldots(3.2)$$

The resulting temperature distribution is given by

$$T = T_0 + \left(\frac{f_c UI}{2\pi K_T r}\right) erfc\left(\frac{r}{2\sqrt{\alpha t}}\right), \qquad \ldots(3.3)$$

At, melt radius *R*,

$$T = T_m = T_o + \left(\frac{f_c UI}{2\pi K_T R}\right) erfc\left(\frac{R}{2\sqrt{\alpha t}}\right), \qquad \ldots(3.4)$$

Here '*R*' is defined as the radius of the crater whose volume is considered to be equivalent to the sum of the crater volumes resulting from several sparks in an actual discharge. PHSM assumes a single spark per discharge pulse, resulting in a

single crater assumed to be of hemispherical shape. The melt cavity volume is approximated to be hemispherical shape. Hence the cathode erosion rate based on a single spark is given by

$$V_w = \frac{V_c}{t_{on} + t_{off}} \quad , \qquad \ldots(3.5)$$

where,

The melt cavity volume $V_c = \frac{2}{3}\pi R^3$ $\qquad \ldots(3.6)$

However, some researchers [4,13] have reported that the number of sparks during a single discharge in EDM or Electro-Chemical Discharge Process is likely to be several, say 3-13.

3.1.2 Procedure used to evaluate theoretical crater volume of the cathode

The theoretical crater volume can be estimated by simultaneously solving Equ.3.4 and Equ.3.6. Equ3.4 is used to calculate of theoretical crater radius (R). In this equation it can be seen that all the parameters are either measured or known except f_c i.e., *the fraction of power lost to the cathode.* U,I,t_{on} and T_o are measured parameters during experimentation and K_T, T_m, C_p and α are the thermo-physical properties.

The average values of thermo-physical properties of the material from room to melting temperature, which are used for the calculation, are given in Table 3.1.

Material	Density (kg/m^3)	Thermal conductivity ($W/m\ ^oK$)	Specific heat ($J/kg\ ^oK$)	Thermal diffusivity ($m^2/sec.$)	Melting temperature (^oK)
Titanium	4500.0	21.9	522.0	9.32×10^{-6}	1953.0
Mild Steel	7545.0	56.1	575.0	12.93×10^{-6}	1808.0
Graphite	1550.0	125.4	709.0	114.1×10^{-6}	2273.0
Copper	8640.0	367.0	438.0	96.98×10^{-6}	1356.0

Table 3.1: Material Properties

The ambient temperature (T_o) of the material is taken as 298 K. Average discharge current (I) is taken as a function of pulse on-time as obtained in Sec. 2.3.2 and 2.4.2.

DiBitonto et.al [5] have assumed that fraction of power going to cathode i.e, f_c is constant for a particular electrode pair and dielectric. They have estimated f_c on the basis of theoretical optimum pulse time from the PHSM with the measured values by AGIE corporation corresponding to 42 μsec pulse time and hence calculated the theoretical optimum pulse times and corresponding erosion rates. The present work proposes f_c to be a function of energy input, which is further justified in Sec. 3.3. Therefore, as a first degree of approximation, a linear variation of f_c with energy input into the system is considered to be applicable.

3.1.3 Calculation of theoretical crater volume for cathode:

Initially, f_c as a linear function of energy input is obtained by calculating f_c from the experimental results, corresponding to the two pulse on-times 10μsec and 200 μsec as explained below.

In actual machining process, multiple sparks per discharge occurs which result in multiple craters. Therefore, for theoretical calculations assume single spark per discharge and hence a single crater is considered. This is taken as the equivalent crater corresponding to the sum of all multiple craters in the actual process. The radius corresponding to this crater is called as the *equivalent crater radius* and the crater volume as *equivalent crater volume.*

Equivalent crater radius (R) for the pulse on-time 10 and 200μsec is obtained by substituting experimental equivalent crater volume, corresponding to these two pulse on-time in Equ 3.6 .The experimental crater volume is given by the product of erosion rate and pulse duration time. These two pulse on times are chosen because the theoretical crater volume is calculated between these two limits and compared with experimental results. Hence f_c is obtained by substituting the obtained equivalent crater radius (R) in Equ 3.4. Since U, I and t_{on} are known at these two points, a linear function of f_c with energy input (U,I,t_{on}) into the system is obtained. This is done for

all the Cases except Cases E and I which had extremely low erosion rates after *20 μsec*. Equations of f_c are given below.

$$\text{(Case A)}\ f_c = 0.0328 + 0.1406\,(U I t_{on}) \quad \ldots(3.7)$$

$$\text{(Case B)}\ f_c = 0.0389 + 0.218\,(U I t_{on}) \quad \ldots(3.8)$$

$$\text{(Case C)}\ f_c = 0.0029 + 0.015\,(U I t_{on}) \quad \ldots(3.9)$$

$$\text{(Case D)}\ f_c = 0.0254 + 0.176\,(U I t_{on}) \quad \ldots(3.10)$$

$$\text{(Case F)}\ f_c = 0.0098 + 0.332\,(U I t_{on}) \quad \ldots(3.11)$$

$$\text{(Case G)}\ f_c = 0.0491 + 0.263\,(U I t_{on}) \quad \ldots(3.12)$$

$$\text{(Case H)}\ f_c = 0.0056 + 0.0175(U I t_{on}) \quad \ldots(3.13)$$

$$\text{(Case K)}\ f_c = 0.0169 + 0.319\,(U I t_{on}) \quad \ldots(3.14)$$

$$\text{(Case J)}\ f_c = 0.0027 + 0.0206\,(U I t_{on}) \quad \ldots(3.15)$$

The crater radius in Cases E and I are so low that the convergence of Equ 3.4 could not be obtained and hence f_c in these cases is not calculated.

Now the theoretical crater radius is obtained for different pulse times to an accuracy of 0.1 *μm* by substituting the obtained f_c as function of energy in Equ 3.4 and hence the theoretical crater volume obtained by substituting the theoretical crater radius (R) in Equ 3.6. This is done for all the cases. The comparisons of theoretical and experimental crater volume of cathode are discussed in Sec 4.2.

3.2 Theoretical estimates of Anode

Anode erosion estimates is based on ECHSM developed by Patel et al. [34] and is discussed below.

3.2.1 Expanding Circular Heat Source Model:

As with the PHSM for the cathode, followings are the main assumptions of expanding circular heat source model (ECHSM):

1. There is one spark per pulse, and the plasma radius at the anode end (a_A at Fig. 1) grows with time as $a = a_0 \times t^{3/4}$.
   - *This is true when power (UI) is constant.*
2. Effective thermo-physical properties of the anodic material apply over the temperature range from solid to liquid melt.
   - *It has been taken for simplicity.*
3. The erosion mechanism is by melting. The initial vaporized cavity resulting from the asymptotic temperature profile (at zero time, r_A and z_A of Fig. 1) is negligible, in term of its contribution to the total volume eroded.
4. A constant fraction f_a of the total power (UI) is lost to the cathode, independent of the current and pulse time. This fraction may change from different dielectric or electrode materials.
   - *No proof is available for its validity.*
5. Heat of fusion of the anodic material is ignored based upon the small differences in erosion rates and times (< 2 %) obtained.

The governing partial differential equation for the determination of the temperature distribution T(r,z.t) due to unsteady-state heat conduction into the anodic material for the anode model is

$$\frac{1}{\alpha}\frac{\partial T}{\partial t} = \frac{\partial^2 T}{\partial r^2} + \frac{1}{r}\frac{\partial T}{\partial r} + \frac{\partial^2 T}{\partial Z^2} \qquad \ldots(3.16)$$

Here $\alpha = \dfrac{K_T}{\rho\, C_p}$ is the thermal diffusivity.

$$\begin{aligned} &IC: t = 0, \quad \text{for all} \quad (z,r),\ T = T_o, \\ &BC: t > 0, \quad -K_T \frac{\partial T}{\partial z} = q(r), \quad \text{for} \quad 0 < r < a(t), \\ &\qquad\qquad -K_T \frac{\partial T}{\partial r} = 0, \quad \text{for} \quad r > a(t), \\ &BC: t > 0, \quad z = r = \infty, \quad T = T_o, \end{aligned} \qquad \ldots(3.17)$$

Where T_0 is the ambient temperature of the solid and K_T is thermal conductivity.

The temperature distribution for a fixed circular disk source is obtained from the analytical solution given by Carslaw and Jaeger [2] as

$$T(r,z,t,r_g)=\frac{r_g\, q}{2K_T}\int_0^{\infty} J_0(\lambda r)J_0(\lambda r_g)\,X\frac{d\lambda}{\lambda}\ , \qquad \ldots(3.18)$$

where λ is dummy variable,

J_0 and J_1 are the Bessel functions of zero and first order, respectively and

$$X=e^{-\lambda z}\ erfc\left(\frac{z}{2\sqrt{\alpha t}}-\lambda\sqrt{\alpha t}\right)-e^{\lambda z}erfc\left(\frac{z}{2\sqrt{\alpha t}}+\sqrt{\alpha t}\right)\ , \qquad \ldots(3.19)$$

Intuitively, it can be seen that the depth to which the melting temperature is reached is maximum at the center, so the solution at $r = 0$ is considered. And the axial temperature at the end of discharge (t) is provided by a much simpler expression, which is derived as a special solution of Equ.3.18 as

$$T(0,z,t)=\frac{2q\sqrt{\alpha t}}{K_T}\left[ierfc\left(\frac{z}{2\sqrt{\alpha t}}\right)-ierfc\left(\frac{\sqrt{z^2-r_g^{\,2}}}{2\sqrt{\alpha t}}\right)\right]\ , \qquad \ldots(3.20)$$

Furthermore, for known power input ($f_a\, U\, I$), the incidence of the energy flux upon the anode is

$$q_A=\frac{f_a UI}{\pi\, r_g^{\,2}(t)} \qquad \ldots(3.21)$$

If Z_m is the depth to which the melting temperature a reached the equation obtained is

$$T_m=\frac{2\,f_a UI\sqrt{\alpha t}}{\pi\, r_g^{\,2}K_T}\left[ierfc\left(\frac{Z_m}{2\sqrt{\alpha t}}\right)-ierfc\left(\frac{\sqrt{Z_m^{\,2}-r_g^{\,2}}}{2\sqrt{\alpha t}}\right)\right]\ , \qquad \ldots(3.22)$$

Where $$ierfc(\zeta)=\frac{1}{\sqrt{\pi}}e^{-\zeta^2}-\zeta erfc(\zeta)$$

$$erfc(\zeta)=1-erf(\zeta)\ ,$$

$$erf(\zeta)=\frac{2}{\pi}\int_0^{\zeta} e^{-x}\,dx$$

The equivalent crater volume V_a for anode as briefly discussed in Appendix B is given by

$$V_a = 1.42898\, Z_m\, r_g^{\,2} \qquad \ldots(3.23)$$

Hence the erosion rate is given by

$$\dot{V}_W = \frac{V_a}{t_{on} + t_{off}} \qquad \ldots(3.24)$$

3.2.2 Procedure used to evaluate crater volume of anode

The theoretical crater volume can be estimated by simultaneously solving Equ3.22 and Equ3.23. Equ3.22 is used to calculate theoretical melting depth Z_m. In this equation all parameters are either measured or known except f_a i.e., *the fraction of power lost to the anode* and crater radius (r_g). Procedure for evaluating of crater radius is given below.

In ECHSM, Patel et al. [34] have assumed that plasma radius at anode end grows with time only as $a = a_o \times t^{3/4}$. They didn't consider the effect of power on plasma radius. For Steel - Copper pair they have taken focus spot growth equation $r_g = 0.788\, t^{3/4} (\mu m)$. But Shankar et al. [37] had shown that current has more dominant effect than pulse on-time as shown in Fig3.2 and Fig3.3. It is also obvious that spark radius should be a function of power (UI).

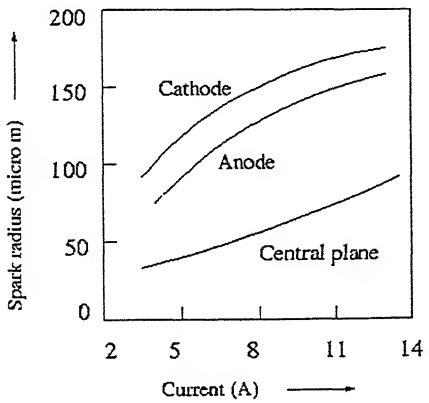

Fig3.2 Effect of current on spark radius at anode, cathode and central plane.[37]

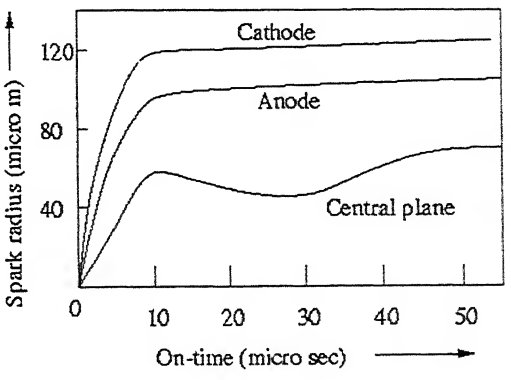

Fig3.3 Spark radius development at anode, cathode and central plane[37].

Erden [8] suggested an empirical relationship to evaluate the radius of a spark for selected pairs of electrodes and dielectric. For rectangular pulse, the radius of discharge is a function of discharge power Q and time (t), written as

$$r_s(t) = KQ^m t^n \qquad \ldots(3.25)$$

Where, $r_s(t)$ is the time function of discharge radius.

Q is the discharge power (UI), t is pulse on-time

and K, m and n are the empirical constants.

Erden [8] had given the numerical values of empirical constants K, m and n for three electrode pairs (Fe, Al and Brass). Discharge length is taken as 10 μm for calculating K. It is observed that these constants vary almost linearly with thermal conductivity K_T, for identical electrode material pairs as shown in Fig 3.4 to 3.6. This logic is extended in the present work for other similar electrode material pairs, but the value of these constants for dissimilar pairs are estimated as the mean of the values for anode and cathode. The calculated values of the constants K, m and n for the selected electrode pairs are given in Table 3.2.

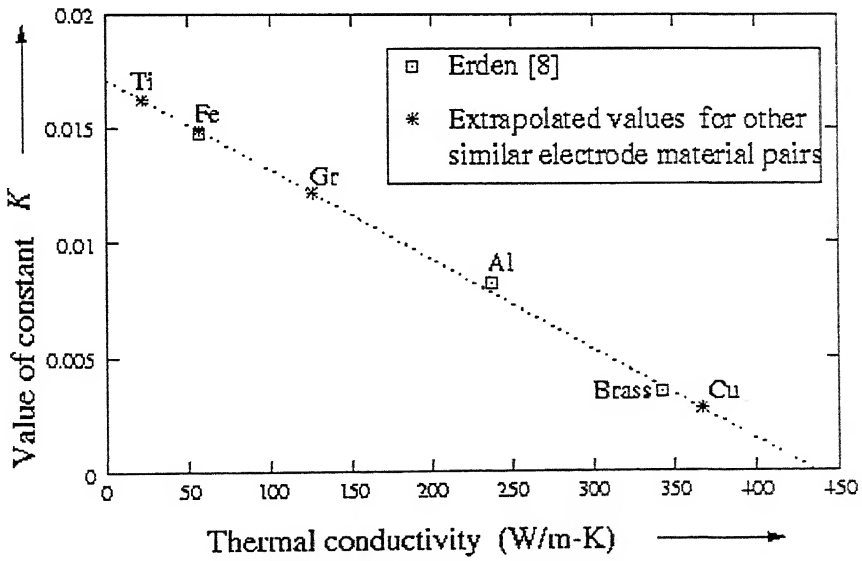

Fig 3.4: Linear variation of empirical constant 'K with Thermal conductivity

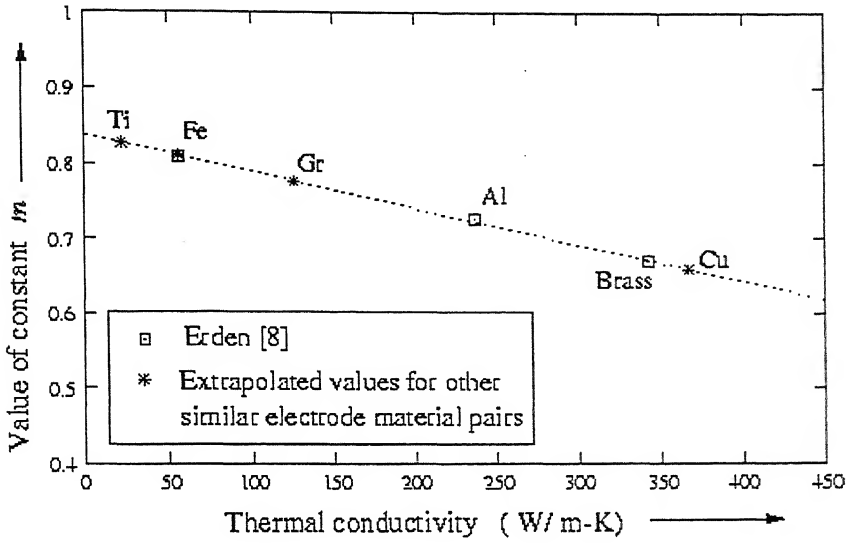

Fig 3.5: Linear variation of empirical constant 'm with thermal conductivity.

Since crater radius is assumed to be equal to the discharge radius [8], Equ 3.25 has been used for calculating the crater radius r_g.

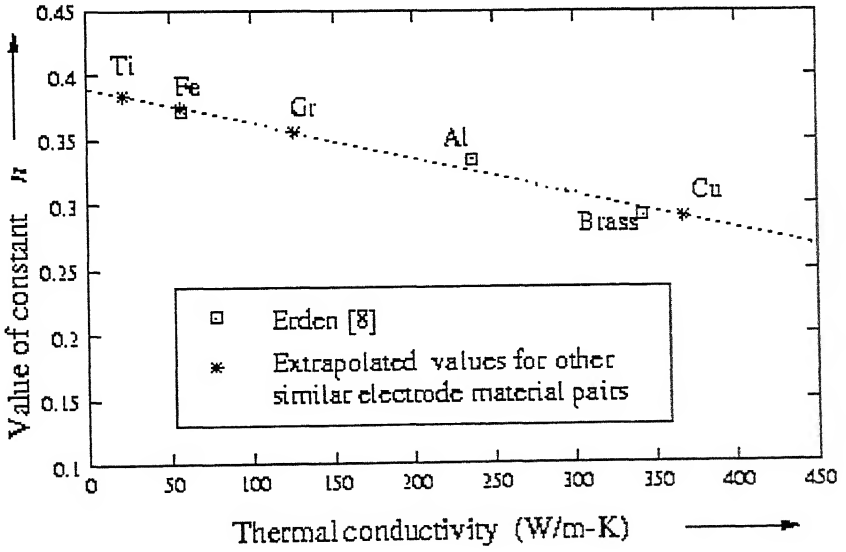

Fig 3.6: Linear variation of constant 'n with thermal conductivity

Patel et al. [34] have assumed that factor f_a is constant for a particular electrode pair and dielectric. But present work proposes f_a as a function of energy input.

Electrode pairs	Thermal conductivity (K_T) ($W/m\text{-}^0K$)	K	m	n
Ti - Ti	21.9	0.01623	0.8269	0.3835
MS-MS	56.1	0.01489	0.8095	0.3710
Gr - Gr	125.4	0.01218	0.7766	0.3554
Cu -Cu	367	0.00275	0.6691	0.2898
Ti -MS	-	0.01556	0.8186	0.3788
Ti - Cu	-	0.00949	0.7434	0.3366
MS - Cu	-	0.00882	0.7347	0.3320
Gr – Cu	-	0.00746	0.7178	0.3226

Table 3.2: The calculated values of empirical constant K, m and n.

3.2.3 Calculation of theoretical crater volume for anode

In this case also, Initially f_a as a linear function of energy input is obtained by calculating f_a from experimental results, corresponding to pulse times 10 μsec and 200 μsec. These two pulse on times are chosen because the theoretical crater volume is calculated between these two limits and compared with experimental results. Crater radius r_g is evaluated from Equ 3.25 for different power and pulse on-time. And depth Z_m is obtained from Equ 3.23 by substituting crater radius r_g and experimental crater volume. Hence f_a is obtained by substituting obtained equivalent crater radius r_g and corresponding crater depth Z_m in Equ 3.22.

Since U, I, t_{on} are known at these two points, a linear function of f_a with energy input (UIt_{on}) into the system is obtained. This is done for all cases except Case E and I and equations of f_a are given below.

$$\text{(Case A)}\quad f_a = 0.127 - 0.621\left(U I t_{on}\right) \qquad \ldots(3.26)$$

$$\text{(Case B)}\quad f_a = 0.135 - 0.305\left(U I t_{on}\right) \qquad \ldots(3.27)$$

$$\text{(Case C)}\quad f_a = 0.0081 + 0.0055\left(U I t_{on}\right) \qquad \ldots(3.28)$$

$$\text{(Case D)}\ f_a = 0.3808 - 12.35\,(U I t_{on}) \quad \ldots(3.29)$$

$$\text{(Case F)}\ f_a = 0.1521 - 0.400\,(U I t_{on}) \quad \ldots(3.30)$$

$$\text{(Case G)}\ f_a = 0.153 - 0.506\,(U I t_{on}) \quad \ldots(3.31)$$

$$\text{(Case H)}\ f_a = 0.1509 - 0.684\,(U I t_{on}) \quad \ldots(3.32)$$

$$\text{(Case J)}\ f_a = 0.0075 + 0.0628\,(U I t_{on}) \quad \ldots(3.33)$$

$$\text{(Case K)}\ f_a = 0.0038 + 0.0237\,(U I t_{on}) \quad \ldots(3.34)$$

The crater radius in Cases E and I are so low that the convergence of Equ 3.22 could not be obtained and hence f_a in these cases is not calculated.

Now the theoretical crater depth Z_m is obtained for different pulse times to an accuracy of 0.1 μm by substituting the obtained f_a as function of energy in Equ 3.22 and obtaining the convergence of different pulse on-time. Hence the theoretical crater volume obtained by substituting the crater radius (r_g) and crater depth Z_m in Equ 3.23. This is done for all the cases. The comparisons of theoretical and experimental crater volume of anode are discussed in Sec. 4.3.

3.3 Justification for variable f_c and f_a as function of energy input:

The distribution of energy into the system elements i.e., cathode, anode and the dielectric in EDM process is very complex [5,7,8,22,34,37]. However a simplified analysis of the process reveals that, for a given energy input per pulse at the inter-electrode gap, the fraction of energy lost to the electrodes depends upon the quantity of energy supplied per pulse at the inter-electrode gap. This is explained as below.

The nature of variation of distribution of energy to the electrodes with the energy supplied per pulse appear to occur in three stages as discussed below and is shown in Fig.3.4.

Stage 1: At lower energies, most of the energy will be lost in ionization, excitation and formation of plasma channel. Therefore the fraction of energy lost to the electrodes will be less.

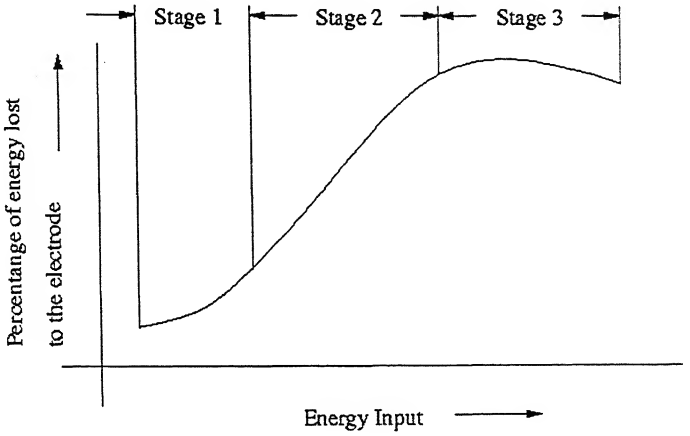

Figure 3.7: Component of energy lost to electrodes.

Stage 2: With further increase in energy at the inter-electrode gap, obviously the energy component conducted into the electrodes will increase.

Stage 3: However a further increase in energy does-not give a significant increase in the fraction of energy conducted to the electrodes because the additional energy supplied will be lost in maintaining the plasma channel, further melting of the molten material, and evaporation of the dielectric fluid [22]. Obviously with further increase in energy, the fraction of energy lost to the electrodes will decrease.

Chapter 4

RESULTS AND DISCUSSIONS

4.1 Average Discharge Current

The variation of average current with pulse on-time during a discharge observed in all the eleven cases (of Table 2.1) are shown in Fig 2.5, 2.22 and 2.23. In all cases, the trend of variation of average current with pulse on-time is similar i.e., it first increases rapidly and after 20 μsec remains nearly constant. On changing the electrode material and polarity of the electrodes, the average current changes, when all other machining conditions are kept same. Hence the energy impressed (UIt_{on}) at the inter-electrode gap depends on the electrode material and the polarity of the electrodes.

Since the average current results due to flow of electrons at the inter-electrode gap, it can be said that *the resistance to the flow of electrons changes with change in electrode material and polarity.*

4.2 Comparison of theoretical and experimental results for cathode erosion

The theoretical crater volume of cathode obtained in Sec. 3.1.3 together with the experimental crater volume cathode for Case A, B, C, D, F, G, H, J, and K are shown in Fig 4.1 to 4.9 respectively. These figures shows that the theoretical crater volumes of cathode calculated using PHSM are closer to experimental crater volume for all cases. This is explained as follows.

It is logical to assume that volume of equivalent crater formed at the electrode will be proportional to the energy impressed at that electrode. And, the energy impressed at an electrode is same as the fraction of total energy at the inter-electrode gap lost to an electrode. This means that the trend of variation of the crater volume

will be similar to that of the variation of f_c with energy input to the system. The experimental crater volume of cathode for all cases almost varies linearly with the given range of pulse on-time except Case C* (MS/MS system in Kerosene) of earlier work [36]. This means that *stage 3* of Fig 3.7 is not reached for the given range of energy input into the system.

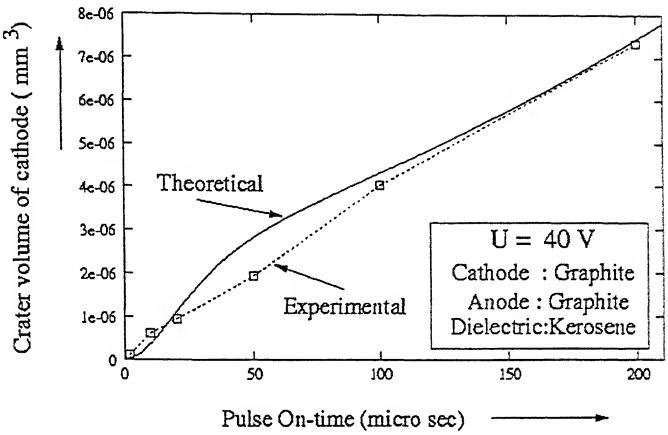

Fig 4.1 Crater volume of cathode for Case A: Gr(-ve)/Gr(+ve) system.

Therefore, variation of f_c with energy input into the system upto the *stage 2* of Fig 3.7 can be considered as a first degree of approximation, to be linear variation. Hence the theoretical crater volume calculated by assuming a linear variation of f_c with energy input into the system which resulted a close agreement to the experimental crater volume.

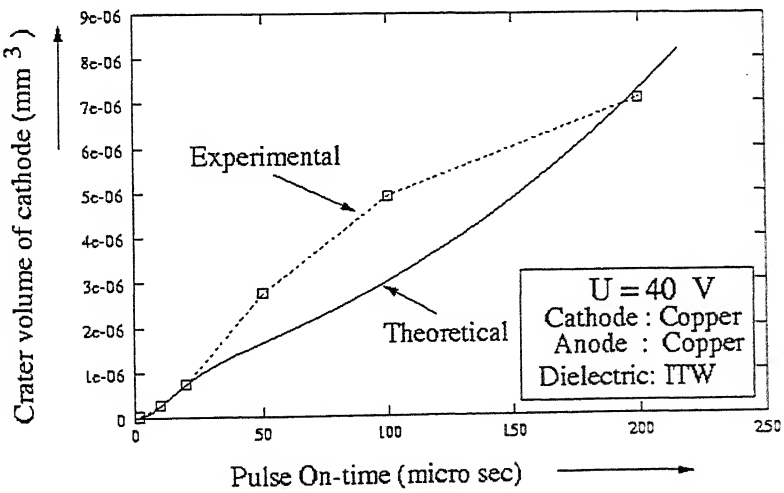

Fig 4.2 Crater volume of cathode for Case B: Cu(-ve)/Cu(+ve) system.

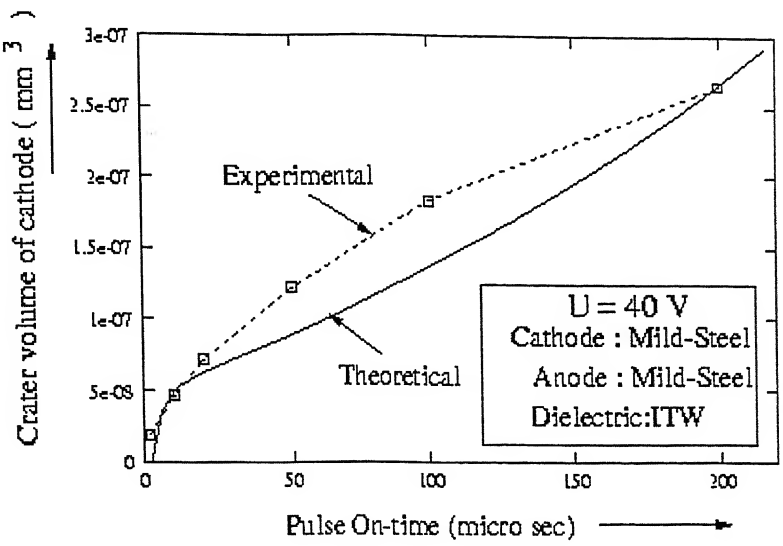

Fig 4.3 Crater volume of cathode for Case C: MS(-ve)/MS(+ve) system.

However in Case C* of earlier study [36], the experimental crater volume increases upto 150 μsec and thereafter it decreases (see Fig C.2) This interprets that the *stage 3* of Fig 3.7 has been reached for the given range of energy input in this case. Therefore it is appropriate to approximate f_c as a second order polynomial of energy input for this case only as shown in Fig C.2.

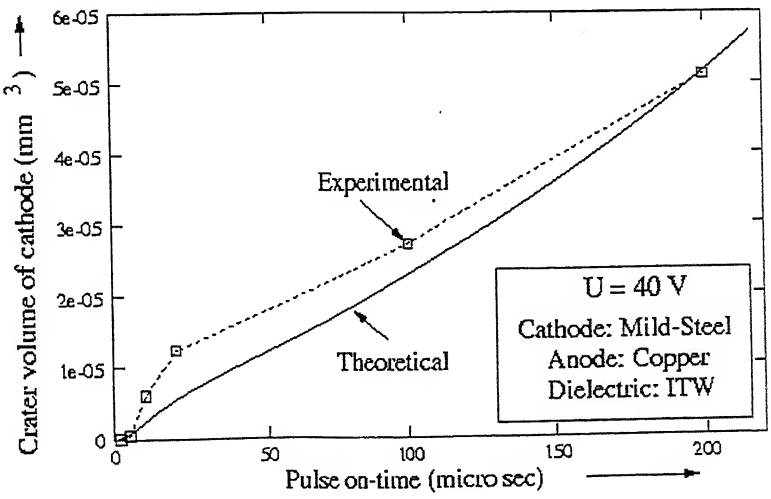

Fig 4.4 Crater volume of cathode for Case D: MS(-ve)/Cu(+ve) system.

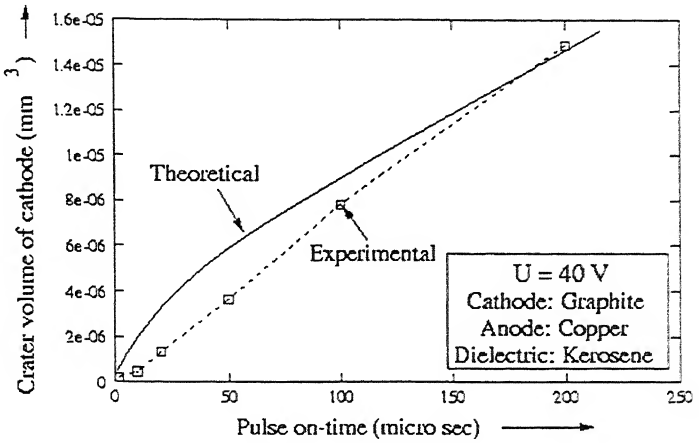

Fig 4.5 Crater volume of cathode for Case F :Gr(-ve)/Cu(+ve) system.

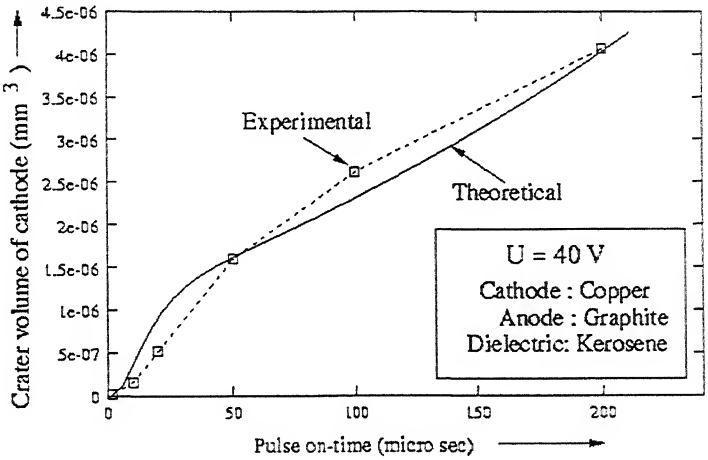

Fig 4.6 Crater volume of cathode for Case G :Cu(-ve)/Gr(+ve) system.

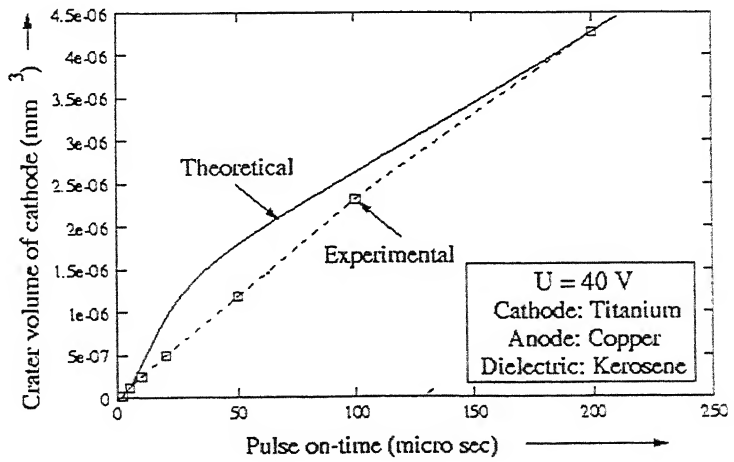

Fig 4.7 Crater volume of cathode for Case H: Ti(-ve)/Cu(+ve) system.

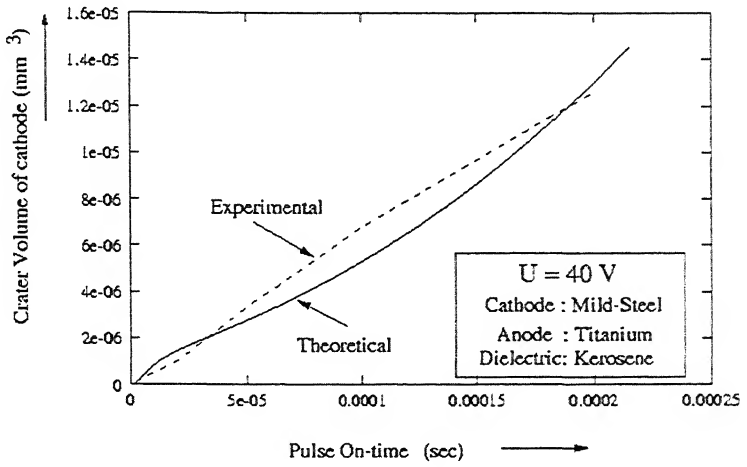

Fig 4.8 Crater volume of cathode for Case J : MS(-ve)/Ti(+ve) system.

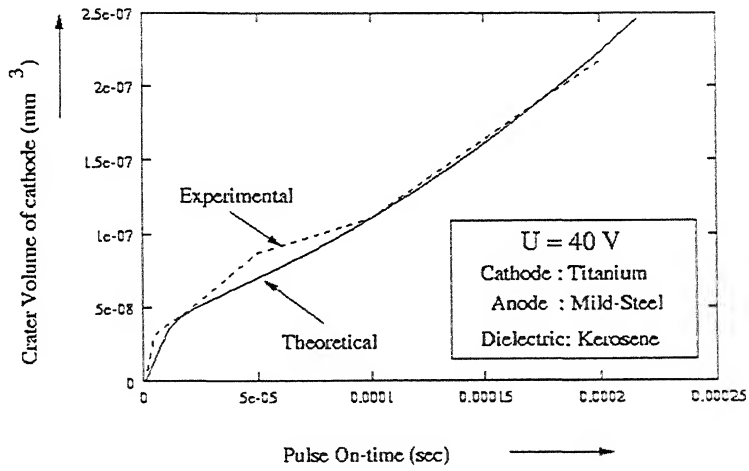

Fig 4.9 Crater volume of cathode for Case K: Ti(-ve)/MS(+ve) system.

4.3 Comparison of theoretical and experimental results for anode erosion

The theoretical crater volume of anode obtained in Sec. 3.2.3 together with the experimental crater volume of anode for case A, B, C, D, F, G, H, J, and K are shown in Fig 4.9 to 4.18 respectively. Like previous section of cathode, these figures also show that the theoretical crater volumes of anode calculated using ECHSM are closer to experimental crater volume. And, explanation is similar to that of cathode of Sec. 4.2.

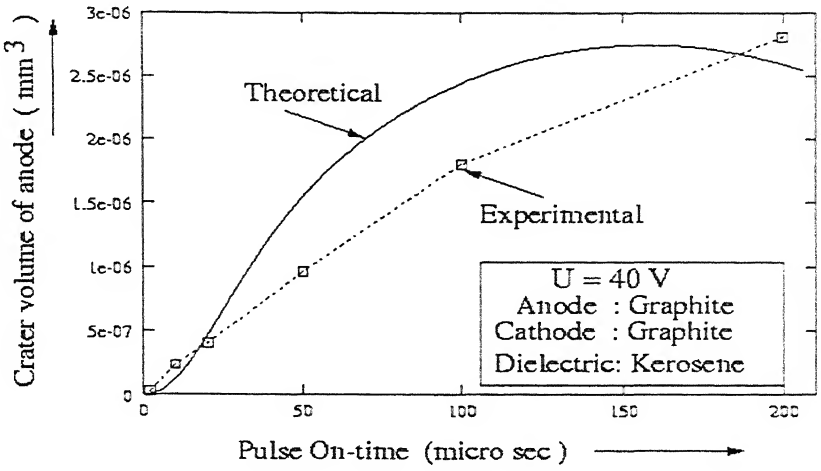

Fig 4.10 Crater volume of anode for Case A :Gr(-ve)/Gr(+ve) system.

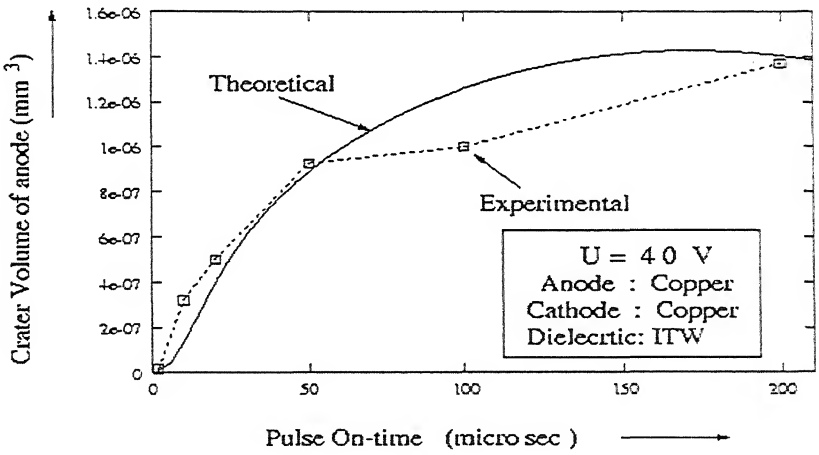

Fig 4.11 Crater volume of anode for Case B :Cu(-ve)/Cu(+ve) system.

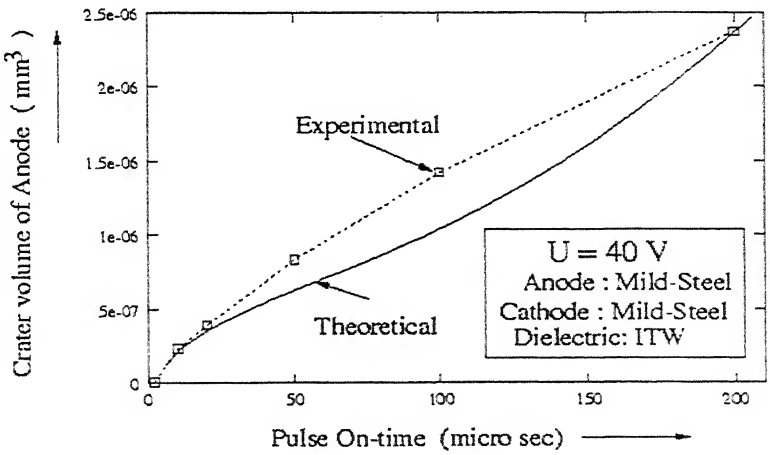

Fig 4.12 Crater volume of anode for Case C: MS(-ve)/MS(+ve) system.

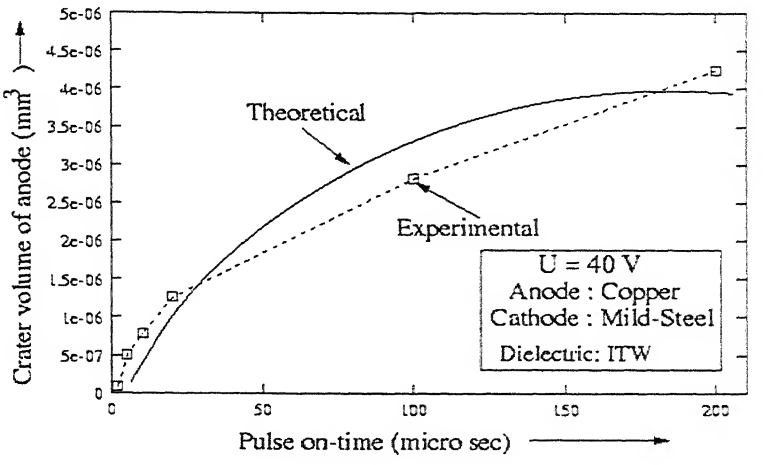

Fig 4.13 Crater volume of anode for Case D: MS(-ve)/Cu(+ve) system.

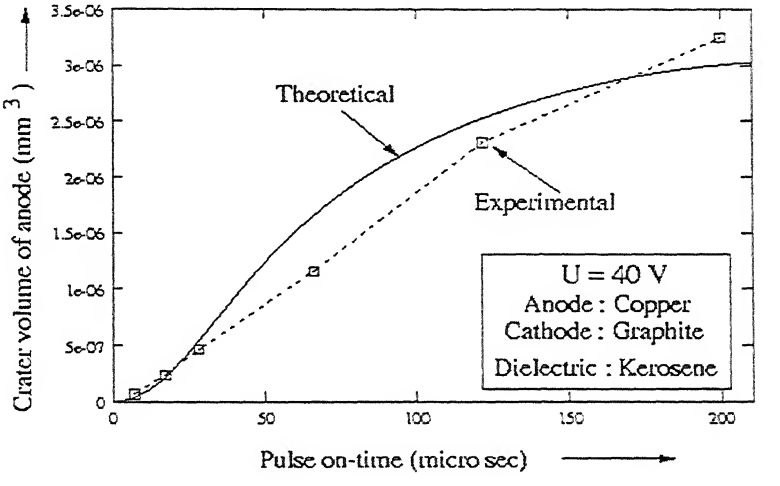

Fig 4.14 Crater volume of anode for Case F: Gr(-ve)/Cu(+ve) system.

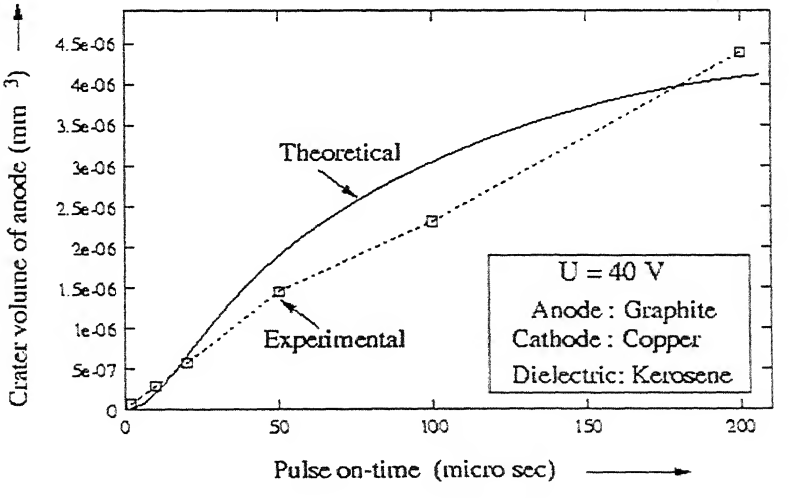

Fig 4.15 Crater volume of anode for Case G: Cu(-ve)/Gr(+ve) system.

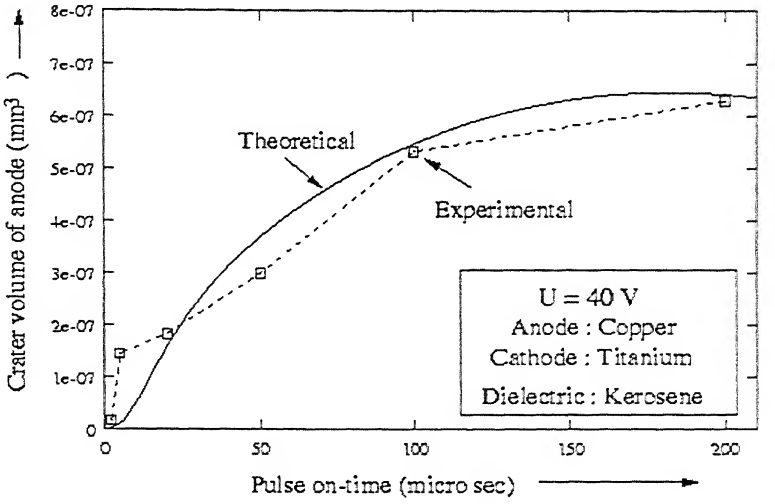

Fig 4.16 Crater volume of anode for Case H: Ti(-ve)/Cu(+ve) system.

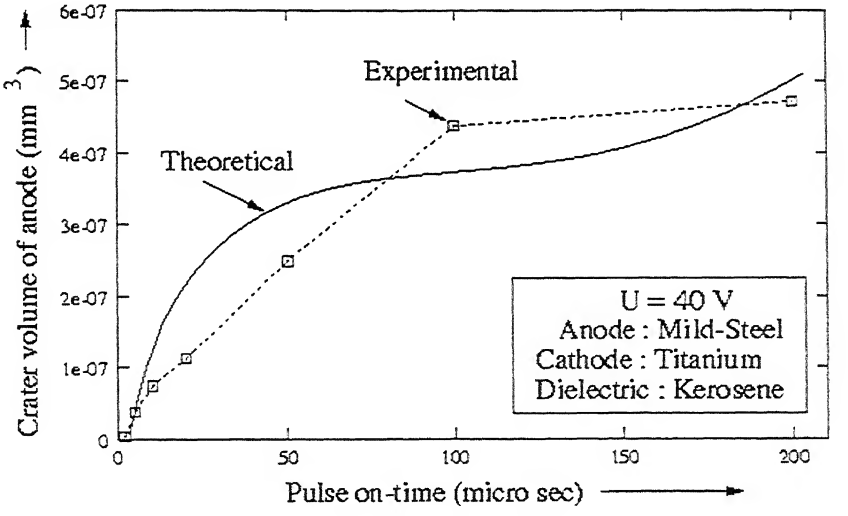

Fig 4.17 Crater volume of anode for Case J: Ti(-ve)/MS(+ve) system.

The experimental crater volume of anode for all cases almost varies linearly with the utilized range of pulse on-time. This interprets that *stage 3* (of Fig 3.7) is not reached for the given range of energy input into the system. Therefore variation of f_a with energy input into the system upto the *stage 2* (of Fig 3.7) can be considered as a first degree of approximation, to be linear variation. Hence the theoretical crater volume of anode calculated by assuming a linear variation of f_a with energy input into the system which resulted a close agreement to the experimental crater volume.

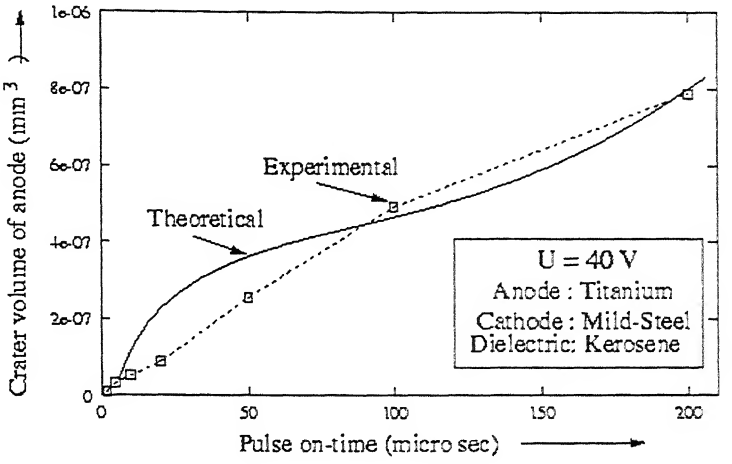

Fig 4.18 Crater volume of anode for Case K: MS(-ve)/Ti(+ve) system.

4.4 Sum of cathode and anode erosion rates.

4.4.1 Similar electrode materials (Case A, B and C)

Fig 4.19 shows variation of the sum of erosion rates of the electrodes (cathode + anode) with pulse energy for the three cases of electrodes of same material system. The trend of sum of electrode rates with pulse energy is similar in three cases i.e., it increases upto certain pulse time (typically 15 *mJ*) and there after it decreases.

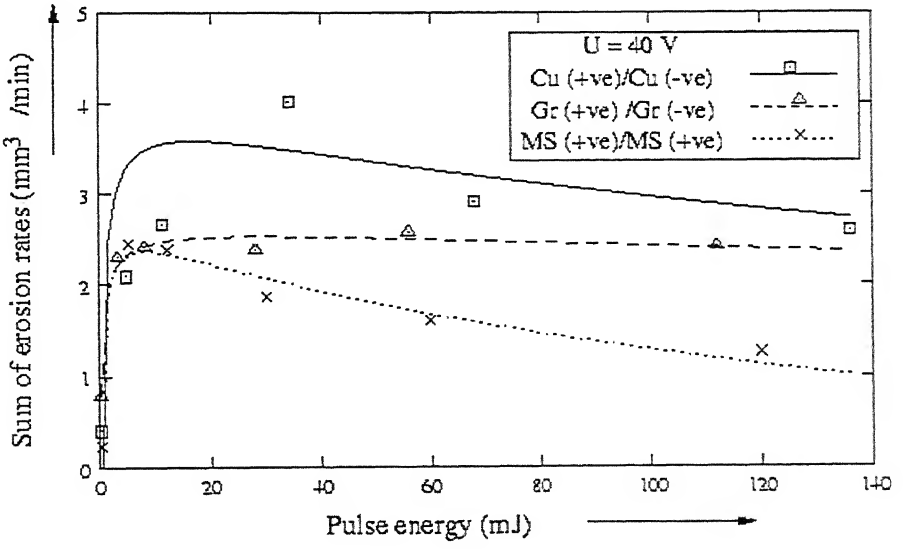

Fig 4.19 Sum of erosion rates of similar electrode material pairs (Case A, B and C)

However it can be seen that sum of erosion rates in Cu/Cu system is highest followed by Gr/Gr system then by MS/MS system. If the models of cathode (PHSM)

and anode erosion (ECHSM) developed by DiBitonto et al. [5] and Patel et al. [34] respectively are accepted to be applicable as stated in Sec 4.2 and 4.3. Then the only possible explanation is that for a given energy input, *the fraction of energy lost to the two electrodes (cathode and anode) is more for Cu/Cu system followed by Gr/Gr system then by MS/MS system*. This can be seen from Equ.3.7, 3.8, 3.9, 3.26, 3.27 and 3.28. The difference in erosion rates is also due to change in the thermal properties of the electrode material.

4.4.2 Dissimilar electrode materials

The variation of the sum of erosion rates of electrodes in Cases D, E, F, G, H, I, J and K (electrodes of dissimilar materials system) with pulse energy are shown in various Figs 4.20 to 4.23. As in earlier cases, the sum of erosion rates of the electrode increases upto certain pulse energy and there after it decreases. In all cases there is huge difference in the sum of erosion rates when the polarity of the electrodes is interchanged as shown in figures. The decrease in sum of erosion rate in Case E i.e., when the cathode is copper and anode is Mild-Steel is very steep after 1.8 *mJ* of energy. But beyond 8 *mJ* the sum of erosion rates is negligible. However in Case D i.e., when the cathode is Mild-Steel and anode is copper, the sum of erosion rates decreases slowly beyond 10 *mJ* as in Fig 4.20.

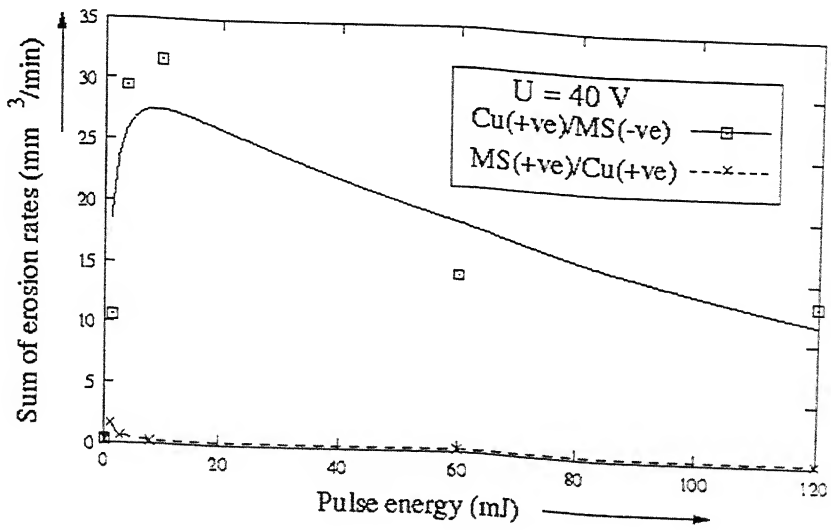

Fig 4.20 Sum of erosion rates of Cu(-ve)/MS(+ve) and MS(-ve)/Cu(+ve)(Case D & E)

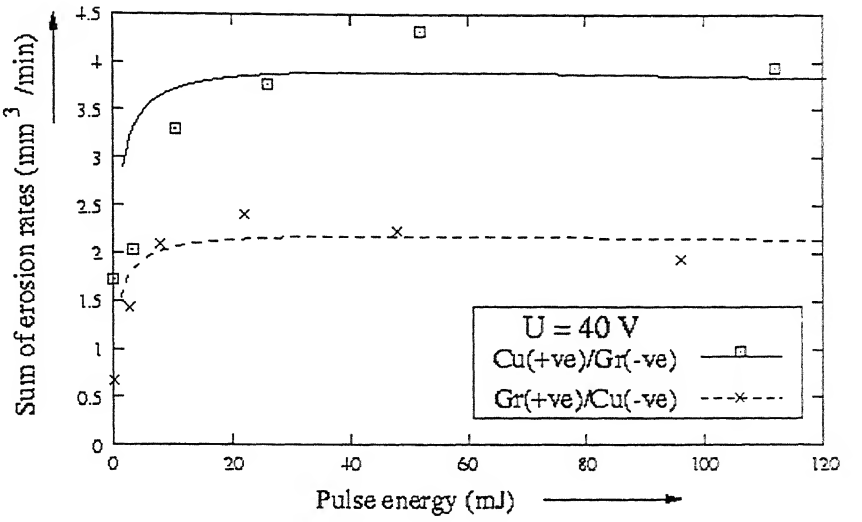

Fig 4.21 Sum of erosion rates of Gr(-ve)/Cu(+ve) and Cu(-ve)/Gr(+ve)(Case F and G)

Fig 4.21 shows the trend of the variation of sum of electrode erosion rates in Graphite and Copper system (Case F and G) which is same for both the cases i.e., first increases upto 20 *mJ* and then nearly constant longer pulse energy. Same trends are also shown in Fig 4.23 for Mild-Steel and Titanium system (Case J and K).

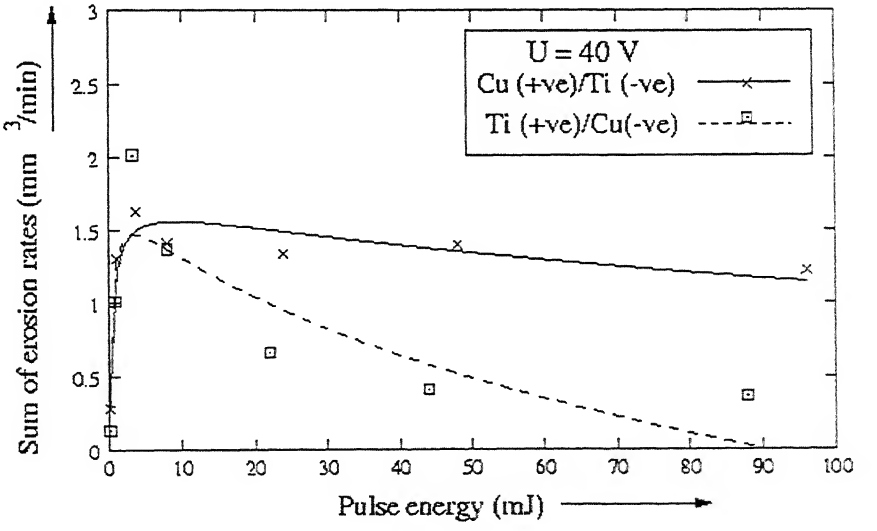

Fig 4.22 Sum of erosion rates of Ti(-ve)/Cu(+ve) and Cu(-ve)/Ti(+ve)(Case H and I).

Fig 4.22 shows the trends of sum of erosion rates with pulse energy in Copper and Titanium system (Case H and I). Effect of polarity is negligible for low pulse energy

(typical upto 5 *mJ*) as in both case the sum of erosion is nearly same. However difference in sum of erosion rates increases with the longer pulse energy.

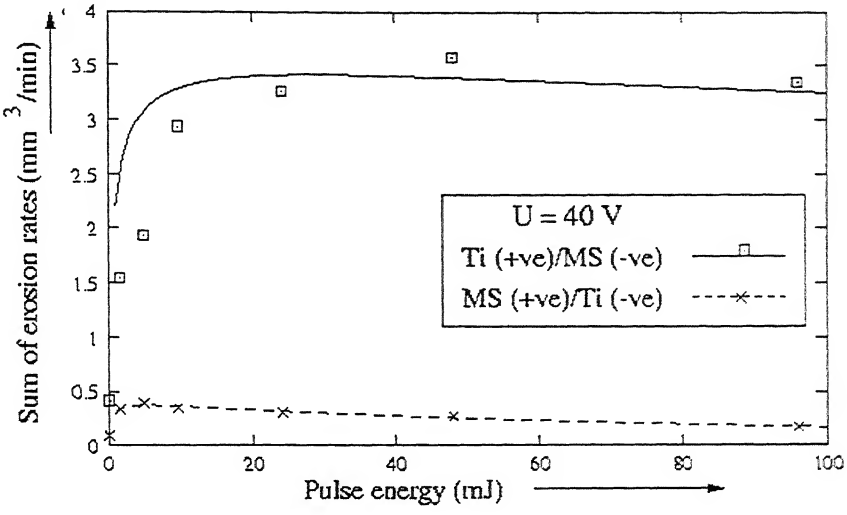

Fig 4.23 Sum of erosion rates of MS(-ve)/Ti(+ve) and MS(-ve)/Ti(+ve)(Case J and K)

In both sections (Sec4.4.1 and 4.4.2), the sum of erosion rates decreases beyond certain pulse energy. This may be due to the following possible reason.

At high pulse energies, in order to keep the breakdown field constant, the electrodes gap spacing increases. This results in higher amount of heat loss, radial diffusion of ions and redeposition between cathode and anode. Therefore the component of energy distributed at the electrodes decreases. Hence the amount of material eroded from both the electrode decreases which results in the decrease in the sum of erosion rates of the electrodes at high pulse energies.

4.5 Polarity Effect

The interchange in polarity of the electrodes has resulted in a huge difference in the erosion rates of the electrodes (see Fig 4.20 to 4.23). The implication of this is as follows.

The energy supplied at the inter-electrode gap is lost into the system elements (i.e., cathode, anode, and dielectric), radiation and some other forms of energy. This can be written as

$$\text{Total energy input} \quad E = E_e + E_w + E_d + E_r$$

$$\Rightarrow \quad 1 = \frac{E_e}{E} + \frac{E_w}{E} + \frac{E_d}{E} + \frac{E_r}{E}$$

$$\Rightarrow \quad 1 = f_e + f_a + f_d + f_r \qquad \ldots(4.1)$$

If material removal from an electrode pair in a given dielectric is independent of the polarity of the electrodes then interchanging the polarity should not alter the sum of erosion rates. But figures in Sec 4.4.2 show clearly that when the polarity of *Cu* is changed, the *total erosion volume changes drastically.* Therefore for MS/Cu system (i.e. Case D and E) from Equ.4.1, we have

$$\text{for Case D,} \quad 1 = (f_e' + f_a') + f_d' + f_r'$$

$$\text{and for Case E,} \quad 1 = (f_e'' + f_a'') + f_d'' + f_r''$$

Concluding from Fig 4.20, therefore

$$(f_e'' + f_a'') < (f_e'' + f_a'')$$

Now, if radiation and other forms of losses which are not accounted for are nearly same in both the cases i.e., $f_r' = f_r''$, then obviously $f_d'' > f_d'$. This implies that more energy is available in the dielectric media. This should result in higher temperature rise of the dielectric in Case E. This investigation was not taken up in the course of present work and is suggested as a follow up task and it is not very simple either.

On the otherhand if the energy lost to the dielectric is same in both the cases then, radiation losses and other losses have to be higher in Case E than in Case D. This aspect can be investigated by resorting to measurement of energy due to ultra-violet, infra-red and visible light in the discharge and would be interesting task.

4.6 Influence of Anode material on the erosion rates of the cathode material

The variation of the erosion rates of the cathode material with different anode material has been studied in four cases as discussed below.

4.6.1 Erosion rate of Copper as cathode material with different anode material

Comparison of Case B, E, G and I

Cathode: Copper

Anode : Copper, Mild-Steel, Graphite and Titanium

From Table 2.1 it can be seen that cathode in Cases B, E, G and I is copper while anode is of copper, mild-steel, graphite and titanium respectively. It can be seen from Fig 4.24 that erosion rate of *Cu* is negligible after 20 and 50 *μsec* when the anode is *MS* and *Ti* respectively. However, beyond that time, erosion rate of cathode (copper) is significantly more when the anode is of copper and graphite. This clearly shows *that the fraction of power lost to the cathode (copper) is much more when the anode is also of copper than all other cases.* Erosion rate of cathode (Cu) is showing two different trends. *One is with anode of Cu and Gr i.e., first increases rapidly then decreases slowly, other is with anode of MS and Ti, where erosion rate first increases rapidly and then decreases drastically between 5 to 50 μsec and thereafter remains almost negligible.*

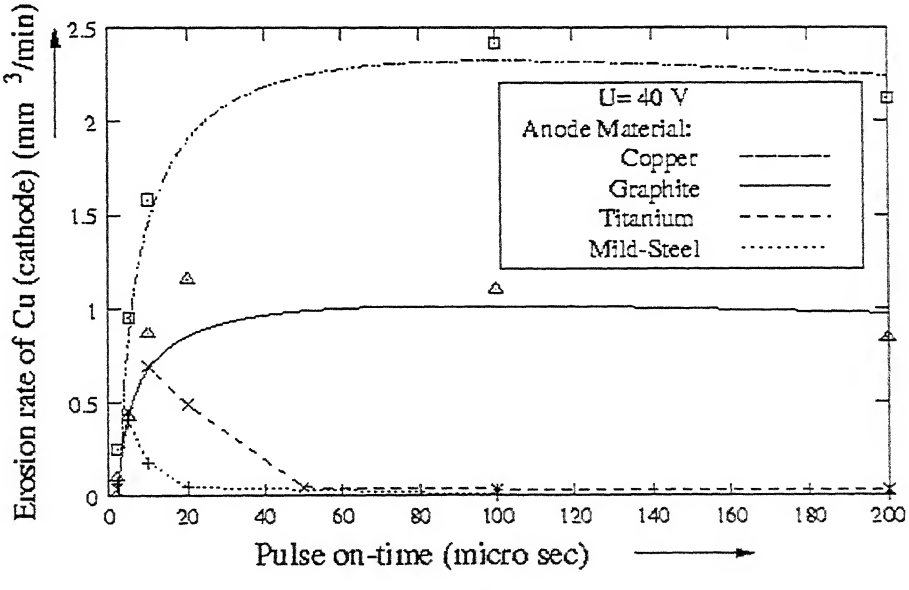

Fig 4.24: Erosion rate of cathode (Cu) when the anode material is Cu, MS, Gr and Ti

The Work-tool erosion ratio (WTER) for Cu cathode decreases when the anode is of MS and Ti (see Fig2.9 and 2.15) whereas it increases when the anode is of Cu and Gr (see Fig 2.2 and 2.13) with pulse on-time. In all the cases (Case B, E, G and I), WTER is less than 1 except Case B i.e., when anode is of copper. In Case B WTER increases rapidly only upto certain pulse on-time and beyond that, the rate of increase is less. *Therefore, for high erosion rate and at the same time maintaining high accuracy of the machining of copper, copper should be preferred over other (MS, Ti and Gr) materials i.e., for anode and machining can be done for a wide range of pulse on-time* (typically 100 to 200 μsec).

4.6.2 Erosion rate of Mild-Steel as cathode material with different anode material

Comparison of Case C, D and K

Cathode: Mild-Steel

Anode : Mild-Steel, Copper and Titanium

From Table 2.1 it can be seen that the cathode material in Case C, D and K is Mild-Steel while the anode is Mild-Steel, Copper and Titanium respectively. In these cases the erosion rate of the cathode is more than the erosion rate of anode (see Fig 2.2, 2.6 and 2.20). The erosion rate of cathode i.e. MS in these combinations of electrode pair is shown in Fig 4.25. It can be seen from the figure that the erosion rates of MS is increased by 12 and 7 times at optimum pulse on-time, when anode material is changed from MS to Cu and Ti to Cu respectively.

This shows that when the anode material is copper, *greater fraction of power is lost to the cathode* (mild-steel) than when anode material is MS or Ti. The mechanism of erosion, energy distribution and dynamics of plasma may not be equally identical. The decrease in erosion rate after the optimum pulse on-time is low in Case C and K, whereas the erosion rate decreases drastically in Case D.

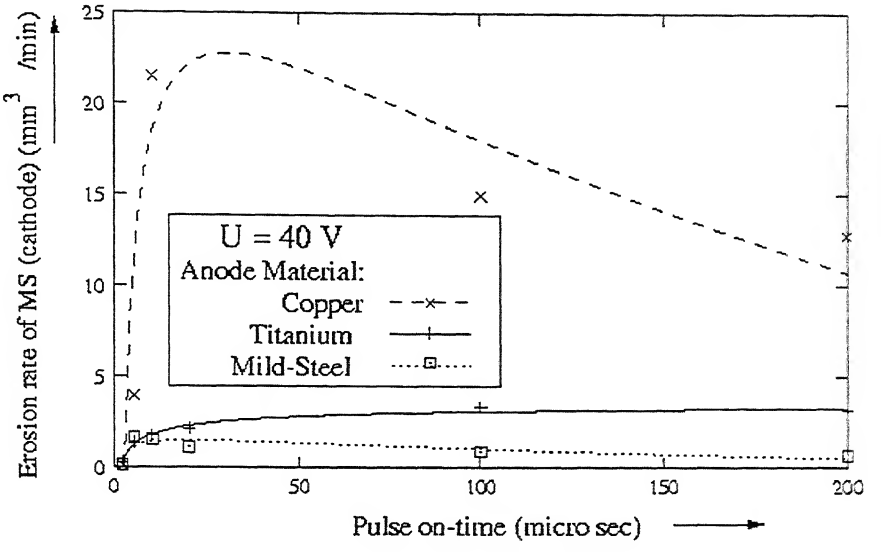

Fig 4.25: Erosion rate of cathode (MS) when the anode material is Cu, MS and Ti

In practice, in addition to maximum material removal rate, the selection of tool depends mostly on WTER. This factor becomes more important when the manufacturing of the tool is very costly or high accuracy of machining i.e., minimum erosion of tool has to be maintained. Hence WTER should be maximum. The WTER is higher for low pulse on-time and has a decreasing trend, when the anode is MS whereas it has an increasing trend when the anode is of Cu and Ti (see Fig 2.2 and 2.21). However, the value of WTER are greater in Case D and K than that in Case C. But in these two case (D and K) erosion rate of mild-steel is more in Case D i.e., when anode is copper. *Therefore where the interest of high erosion rate of MS, Cu should be preferred. And for high accuracy machining, Titanium should be preferred to as anode (tool) and machining is done for higher pulse on-times.*

4.6.3 Erosion rate of Graphite as cathode material with different anode material

Comparison of Case A and F

Cathode: Graphite

Anode: Graphite and Copper

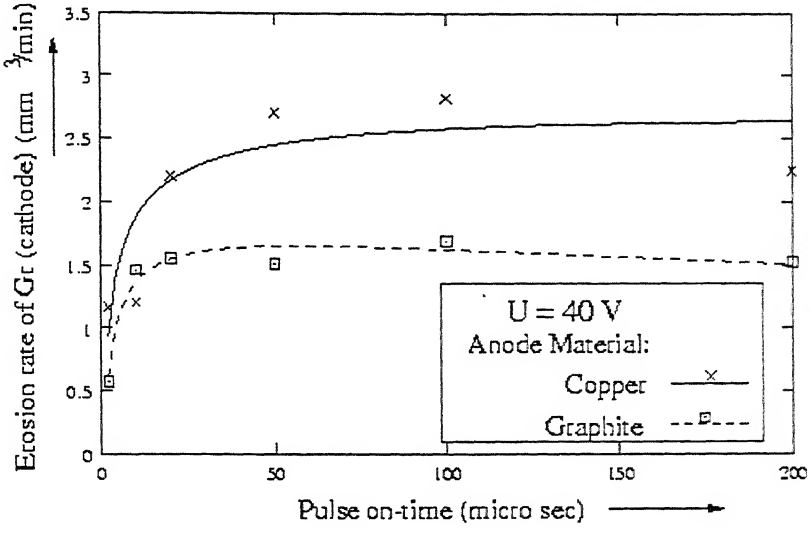

Fig 4.26: Erosion rate of cathode (Gr) when the anode material is Cu and Gr

From Table 2.1 it can be seen that the cathode material in Case A and F is Graphite when the anode is of Graphite and Copper respectively. In both the case erosion of cathode is more than anode (see Fig 2.1 and 2.10). The erosion of cathode graphite with these combinations of electrode pair is shown in Fig 4.26. It can be seen from this figure that erosion rate of cathode (Gr) is increased by 1.7 times at the optimum pulse on-time when anode material is changed from Gr to Cu.

As before, it shows that when the anode material is copper, greater fraction of power lost to cathode (Gr) than when anode material is Gr. For Case F i.e., when copper is of anode, erosion rate of cathode as well as WTER is more than Case A for longer pulse on-time. So copper should be preferred as tool for these cases.

4.6.4 Erosion rate of Titanium as cathode material with different anode material

Comparison of Case H and K

Cathode: Titanium

Anode: Copper and Mild-Steel

From table 2.1 it can be seen that the cathode material in case H and K is titanium while the anode material is Cu and MS respectively. The erosion rates of cathode i.e., Ti in these combinations of electrode pairs as shown in Fig 4.27. It is clear from the figure that erosion rate of titanium is increased by 10 times at optimum pulse on-time, when anode material is changed from mild-steel to copper. By considering higher erosion rate as well as WTER copper is preferred for machining of Ti in longer pulse on-times.

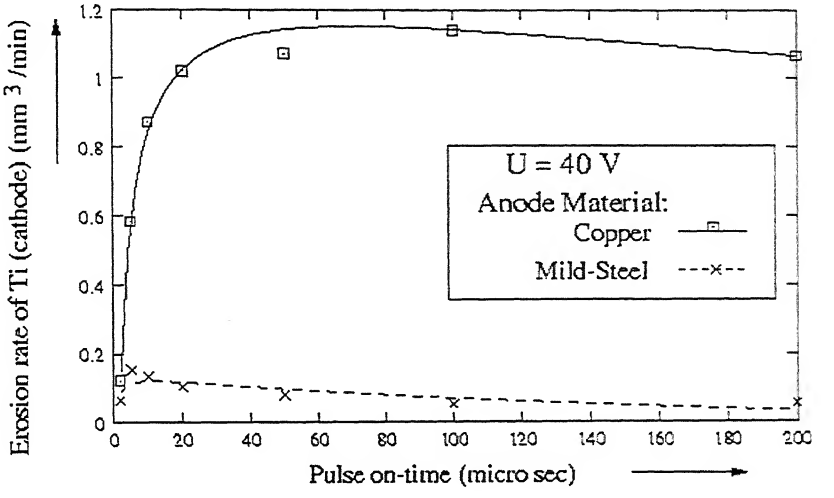

Fig 4.27: Erosion rate of cathode (Ti) when the anode material is Cu and MS.

From discussion in Sec 4.6.1, 4.6.2, 4.6.3 and 4.6.4, it can be said that by changing the anode material, the erosion rates of the cathode can be changed drastically. Copper as anode results in *greater fraction of power lost to the cathode* (Cu, MS, Gr and Ti) when compared to MS, Gr and Ti as anode. This brings out significant role of copper as an electrode. Besides the usual thermal properties of copper, its fundamental electronic properties like work function, emissivity etc may be of significance. This could influence the erosion mechanism. Therefore the economical machining (i.e., high material removal rate) of work-piece (Cu, MS, Gr and Ti) the work-piece should be connected to the cathode and tool (anode) is preferred of copper.

Chapter 5

CONCLUSIONS

5.1 Conclusions

In the present work, electric discharge machining on eleven sets of electrode pair (shown in Table 2.1) has been carried out and the following conclusions have derived.

1. The PHSM and ECHSM have been studied with the experimental results for eleven sets of electrode pair. It has been concluded that the above two model can be used to estimate the cathode and anode erosion in EDM process with the fair degree of accuracy, provided it is assumed that the fraction of energy going to the electrode is a function of energy input into the system.
2. In similar tool/work electrode pairs, cathode erosion rate is higher than anode erosion rate for the range of pulse on-time utilized. Hence for higher work-tool erosion ratio, work should be made cathode in EDM die-sinking operation.
3. In similar tool/work electrode pair greater component of pulse energy is distributed to the electrodes in the Cu(-ve)/Cu(+ve) system than MS(-ve)/MS(+ve) and Gr(-ve)/Gr(+ve) systems. This suggests that the loss of energy into the dielectric and other forms of radiation energy such as ultra-violet, infra-red and visible light etc. is less in Cu(-ve)/Cu(+ve) system.
4. In dissimilar tool/work electrode pair, the polarity of the electrodes has a significant effect on the distribution of energy in the system elements. As the interchange in polarity has resulted a huge difference in the sum of erosion rates of electrode. The energy transmitted to the electrodes in MS(-ve)/Cu(+ve) system is significant than that in Cu(-ve)/Ms(-ve) system. Hence it has been concluded that the energy lost into the dielectric will be more in Cu(-ve)/MS(+ve) system than in MS(-ve)/Cu(+ve) system. This may result in much increase in temperature of the dielectric in Cu(-ve)/MS(+ve) system than in MS(-ve)/Cu(+ve) system.

5. The study has shown that an electrode (anode or cathode) has significant effect on the distribution of energy at the other electrode (cathode or anode). The erosion rate from cathode of MS, Cu, Gr and Ti gives always higher erosion rates when copper is used as anode in comparison to MS, Gr and Ti anodes. This shows that copper anode is showing special characteristics in controlling the cathode erosion as compared to others.

5.2 Scope Of future work

1. The temperature of the dielectric can be investigated for different polarities of an electrode pair. Hence the component of energy lost into the dielectric and in other forms of energy such as ultra-violet, infra-red radiation and visible light etc can be obtained.
2. The electrode material properties which influence the distribution of energy into the electrodes with change in polarity has to be studied. Then a theoretical model can be developed to obtain the fraction of power distributed at the electrodes as a function of energy input into the system, polarity of the electrodes and electrode material properties.
3. Development of comprehensive analytical model to find the fraction of energy going to cathode, anode and dielectric based on discharge phenomenon is still required.

REFERENCES

1. Alinski Kazimiez, (1995), "*The polarity of electrodes in Electro Discharge machining*", Proceedings International symposium for Electro machining – *XI*, pp.95-10.
2. Carslaw M.S. and J.C. Jager, *Conduction of heat in Solids*, Oxford press, Oxford (1959).
3. Crookall J.R. and C.J.Heuvelman, " *Electro-Discaharge Machining - the state of art*", XXI General Assembly of CIRP, CIRP, Poland, 1971, pp. 113-120.
4. Dharmadhikari S.W. and C.D.Sharma, (1980), "*Determination of material removal in EDM using a multiple heat source model*", Proceedings of the 9th AIMTDR conference IIT Kanpur.
5. DiBitonto Daryl D., Philip T.Eubank, Mukund R.Patel and Maria A.Barrufet,(1989), "*Theoretical models of the Electrical Discharge machining process –I. A simple Cathode Erosion model*", J. Appl. Phys., 66(9), 1, pp.4095-4103,
6. Dijck F.S. Van and W.L. Dutre, "*Heat Conduction model for the calculation of volume of molten metal in electric discharge*", J. Phys. D: Appl. Phys., Vol. 7,1974, pp.898-910.
7. Erden A. and B.Kaftanoghi, (1981), "*Thermo-Mathematical modeling and optimization of Energy pulse forms in Electric Discharge Machining (EDM)*", Int. J. Mach. Tool Des. Res., Vol 21, No. 1, pp.11-22.
8. Erden A., (1983), "*Effect of materials on the mechanism of Electric Discharge machining (EDM)*", Transactions of the ASME, Vol.105, pp.132-138.
9. Erden A., Faruk Arinc and Murat Kogmen, "*Comparison of Mathematical models for Electric Discharge Machining*", Journal of Materials Processing & Manufacturing Science, Vol. 4, Oct. 1995, pp. 163-176.
10. Eubank Philip T., Mukund R. Patel, Maria A. Barrufet and Bedri Bozkurt, "*Theoretical models of the Electrical Discharge machining process – III. The Variable Mass, Cylindrical Plasma model*", J. Appl. Phys., 73 (11), 1 June, 1993 pp. 7900-7909.

11. George V. and V.C.Venkatesh, (1980), "*Investigation on Optimum machining conditions for Electro-Discharge machining of 5Cr Die steel*", Proceedings of the 9th AIMTDR Conference IIT-Kanpur, pp.327-332.
12. George V., P.K.Philip, (1978), "*Analysis of EDM performance and tool wear in Cu-Die steel system – a review*", Proceedings of the 8th AIMTDR Conference I.I.T.,Bombay, pp. 521-525.
13. Ghosh A., M.K.Muju, S.Parija & A. Kanjrathinkal, (1997), "*Microwelding using Electrochemical Discharge*", Int. J. Mach.Tools Manufact. Vol 37, No.9, pp.1303-1312.
14. Guerrero-Alvarez J.L., J.E. Greene and B.F. Von Turkovich, "*Study of the Electro-Erosion phenomemon of Fe and Zn*", Journal of Engineering for Industry, Nov. 1973, pp. 965-971.
15. Heng XI A, Masaneri Kunieda, "*Research on machining characteristics of polarity changed pulse in EDM*," Proceeding International Symposium for Electro Machining- XI, pp.181-190.
16. Heuvelman C.J.,H.J.A Horsten and P.C. Veenstra, "*An Introductory Investigation of the Breakdown Mechanism in Electro-Discharge Machining*", Annals of CIRP,1971.
17. Jaswani M.L., " *Effect of the Addition of Graphite powder to Kerosene used as dielectric fluid in Electrical Discharge Machining*", Wear, 70, 1981, pp. 133-139.
18. Jaswani M.L., " *Electrical Discharge Machining in Distilled water*", Wear 72 (1981) pp. 81-88.
19. Jilani S.T. and P.C. Pandey, " *An analysis of surface erosion in Electrical Discharge Machining*", Wear, 84 (1983) pp. 275-284.
20. Jilani S.T. and P.C. Pandey, " *Analysis and Modeling of EDM parameters*", Precision Engineering 1982, pp. 215-221.
21. Jilani S.T. and P.C. Pandey, "*Experimental investigation into the performance of water as a dielectric in EDM.*", Int. J. Mach. Tool Des. Res. Vol. 24, No. 1, pp. 31-43, 1984.
22. Konog M., R.Wertheim, Y.Zvirin and M.Toren, (1997), "*Material Removal and Energy Distribution in Electrical Discharge Machining*", Annals of the CIRP, Vol.24/1, pp.95-100.

23. Lazarenko B.R., (1964), "*The present state of development of Electrospark machining of Conductive materials abroad*", Electro Spark Machining of Metals, Vol.2, edited by B.R.Lazarenko, (Consultants Bureau, Newyork, 1964), pp.181-195.

24. Lonardo P.M. and A.A. Bruzzone, " *Effect of flushing and electrode material on Die Sinking EDM.*", CIRP Vol. 48/1, 1999.

25. Longfellow J., J.D.Wood and R.B.Palme, (1968), "*The effects of Electrode material properties on the wear ratio in Spark-Machining*", Journal of the Institute of metals, Vol.96, pp.43-48.

26. Marty C.C and M. Laracine "*Accuracy of Physico-mathematical Analysis in EDM process- correlation with electrode tool wear*", CIRP 1977.

27. Marty C.C, " *Investigation of surface temperature in Electro-Discharge Machining*", Trans of ASME, Aug 1977, pp. 682-684.

28. McGeough J.A. ,H.Rasmussen, (1982), "*A macroscopic model of Electro Discharge machining*", International J. Mach. Tool Des. Res., Vol. 22, No. 4, pp.333-339.

29. Pandey P.C. and H.S. Shan, *Mordern Machining process*, Tata McGraw-Hill, New Delhi, pp.97.

30. Pandey P.C. and S.T.Jilani, (1986), "*Plasma channel growth and the resolidified layer in EDM*", Precision Engineering, Vol.8, No.2, pp. 104-109.

31. Pandit S.M. and K.P. Rajurkar, "*Crater Geometry and the volume from Electro-Discharge Machined Surface profiles by Data Dependent System*", Trans of ASME, J. of Engineering for Industry Nov 1980, Vol 120 pp. 289-295.

32. Pandit S.M. and K.P.Rajurkar, (1983), "*A stochastic approach to thermal modeling applied to Electro-Discharge Machining*," Journal of heat transfer, vol 105 , pp.555-562.

33. Pandit S.M.and K.P.Rajurkar, (1980), "*Data Dependent Systems Approach to EDM process modeling from Surface Roughness profiles*", Annals of CIRP,Vol.29/1, pp.107-112

34. Patel Mukund R., Maria A.Barrufet , Philip T.Eubank and Daryl D.DiBitonto, (1989), "*Theoretical models of the Electrical Discharge machining process – II. The Anode Erosion model*", J. Appl. Phys., 66(9), 1, pp.4104-4111.

35. Roethel F., L. Kosec, V. Garbajs and J.Pekienik, "*Contribution to the Micro-Analysis of the Spark Eroded Surfaces*", Annals of the CIRP, Vol. 25/1/1976, pp. 135-140.
36. Saha Ranjit, (1999) "*An investigation into the tool-work polarity effects on mutual erosion rates in EDM process*", M.Tech Thesis, IIT Kanpur , India.
37. Shankar P.,V.K.Jain and T. Sundararajan, (1997), "*Analysis of spark profiles during EDM process.*", Machining science and Technology, 1(2),195-217.
38. Singh A. and Amitabh Ghosh, " *A thermo-electric model of material removal during electric discharge machining*", Int. J. of Mach. Tool & Manufacture, Vol. 39, 1999, pp. 669-682.
39. Snoeys R., H. Cornelissen and K.U. Leuven, "*Correlation between Electro Discharge machining data and machining settings*", Annals of the CIRP, Vol. 24/1/1975, pp. 83-88.
40. Vaseekaran S. and C.A.Brown, (1996), "*Single discharge, spark erosion in TiB_2 and Zinc Part I: Experimental*", Journal of Materials Processing Technology, Vol.58, pp.70-78.

Appendix A

CLIBRATION CHART FOR R-35 GENERATOR

t_{on} (μsec)→	2000	1000	500	200	150	100	50	20	10	5	2	1
τ ↓ Position												
1	2600	2600	1500	600	440	260	230	117	73	45	27	14
2	2600	1940	1000	390	345	194	135	71	49	37	23	13
3	2600	1500	750	300	245	150	101	51	40	31	19	12
4	2350	1160	600	233	175	117	79	41	32	26	17	11
5	1850	920	460	180	140	92	66	34	27	23	15	10
6	1450	720	360	140	120	72	51	27	21	19	12	9
7	1125	565	280	110	90	56	41	21	17	16	11	9
8	860	440	214	90	70	43	31	16	13	12	9	7
9	640	320	160	60	60	32	22	12	10	10	7	6
10	440	220	110	40	40	22	16	8	7	7	5	5
11	270	130	70	30	32	14	10	5	5	5	3	3
12	130	60	30	10	10	6	5	3	2	2	2	2

The values against τ position is the pulse off-time for the corresponding pulse on-time.

Appendix B

Crater Geometry and Volume for anode

Hemi-spherical crater shape considered for the cathode erosion model as it is based on the pointed heat source, but this approximation is not valid for the anode model as it is based on expanding circular heat source. It was found [31,32] that the isothermal curves obtained for the thermal models for circular heat source can be approximated by an exponential function.

$$y = A\, e^{-px} \qquad \ldots(B.1)$$

Where A and P are constants

and x and y are variables.

Therefore, the exponential shape of the Green's function can be considered to be representing a half of section of a characteristic crater in two dimensions Fig.B.1. The three dimensional crater can be obtained by rotating the exponential around a suitable vertical axis as the EDM surface is known to be isentropic. Since the exponential doesn't mathematically becomes zero until infinity, it is necessary to select some finite large value of its arguments to represent the bottom of the crater. By selecting 4.5 times constants, the response reduces to 1 percent to initial value (actually $e^{-4.5} = 0.0111089$). The cut off at $4.5/p$ leads to better predications of erosion volume.

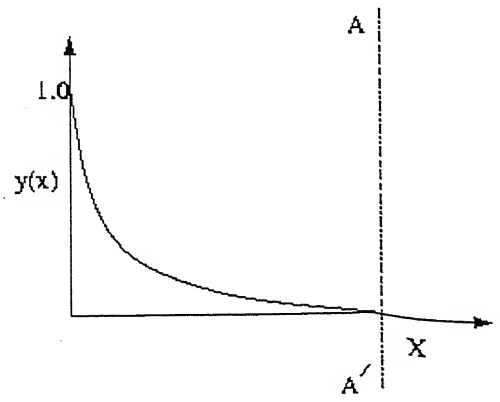

Fig B.1 Exponential curve.

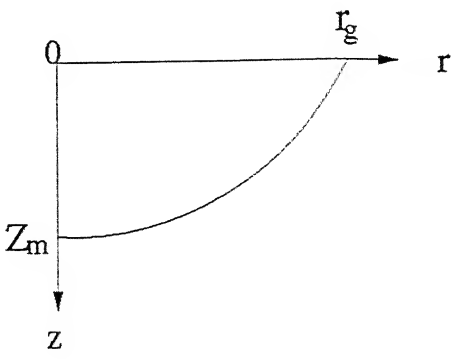

Fig B.2 Exponential crater profile.

The equation of the characteristic crater curve shown in Fig B.2 can be obtained [32] as

$$z = Z_m \left\{ 1 - e^{-4.5\left(1-\frac{r}{r_g}\right)} \right\} \qquad \ldots(B.2)$$

Z_m is crater depth.

r_g is crater radius.

The volume of solid generated by revolution of the area bounded by the above exponential curve about z-axis can estimated by ordinary integration is given as

$$V_c = \pi \int_{z_1}^{z_2} r^2 \, dz \qquad \ldots(B.3)$$

Now at

$$\begin{aligned} r_1 &= r_m \qquad z_1 = 0 \\ r_2 &= 0 \qquad z_2 = \left(1 - e^{-4.5}\right) Z_m \quad = 0.9888\, Z_m \end{aligned} \qquad \ldots(B.4)$$

Therefore

$$V_c = \pi \int_0^{0.9888 Z_m} \left[\frac{r_g}{4.5} \ln\left(1 - \frac{z}{Z_m}\right) + 4.5 \right]^2 dz \qquad \ldots(B.5)$$

The above integral reduces to

$$V_c = 1.42898\, Z_m\, r_g^{\,2} \qquad \ldots(B.6)$$

Equ B.6 has been used for the present work for calculating crater depth Z_m by substituting experimentally evaluated crater volume V_c and crater radius r_g.

Appendix C

Selected graphs of Reference No. [36]

C.1 Comparison of theoretical and experimental results for cathode

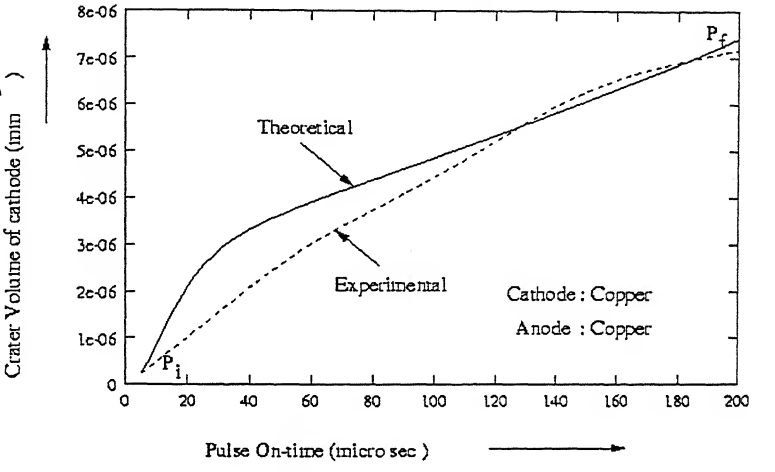

Fig C.1 Crater volume of cathode (Cu) for Cu(-ve)/Cu(+ve) system(Case B*)

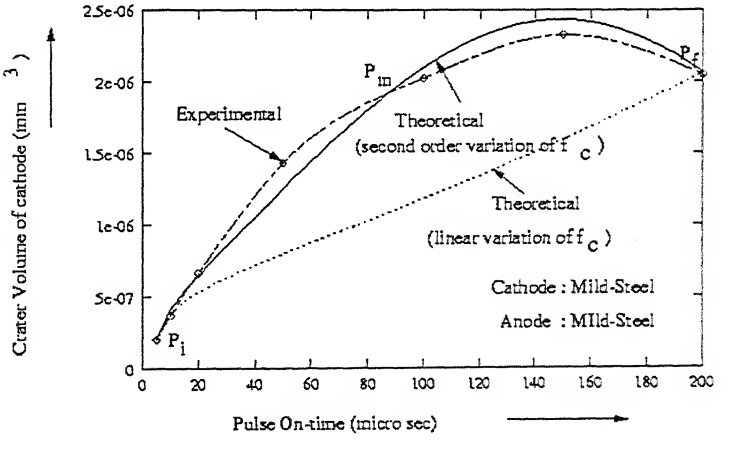

Fig C.2 Crater volume of cathode (MS) for MS(-ve)/MS(+ve) system(Case C*)

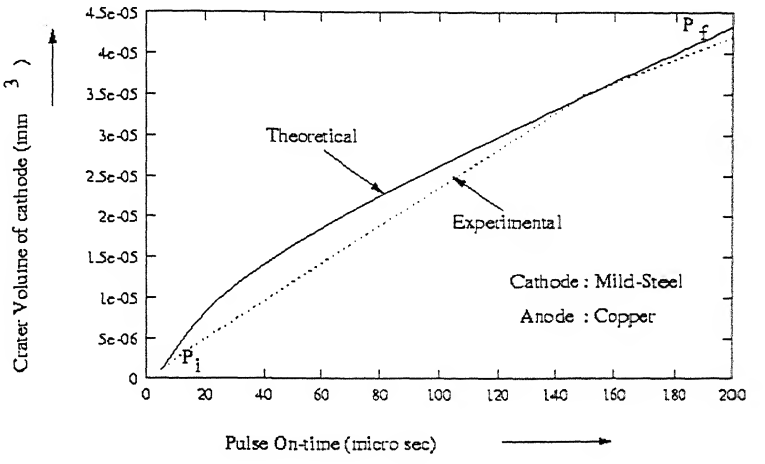

Fig C.3: Crater volume of cathode (MS) for MS(-ve)/Cu(+ve) system(Case D*)

The *fraction of power going to cathode* i.e., f_c as a function of energy for Case B*, C* and D* of Table 2.1 as given below.

$$f_c \text{ (Case B}^*\text{)} = 0.0464 + 0.111\ (UIt_{on}) \quad \ldots(C.1)$$

$$f_c \text{ (Case C}^*\text{)} = 0.0068 + 0.025\ (UIt_{on}) \quad \ldots(C.2)$$

$$f_c \text{ (Case D}^*\text{)} = 0.0329 + 0.065\ (UIt_{on}) \quad \ldots(C.3)$$

C.2 Sum of electrode erosion rate

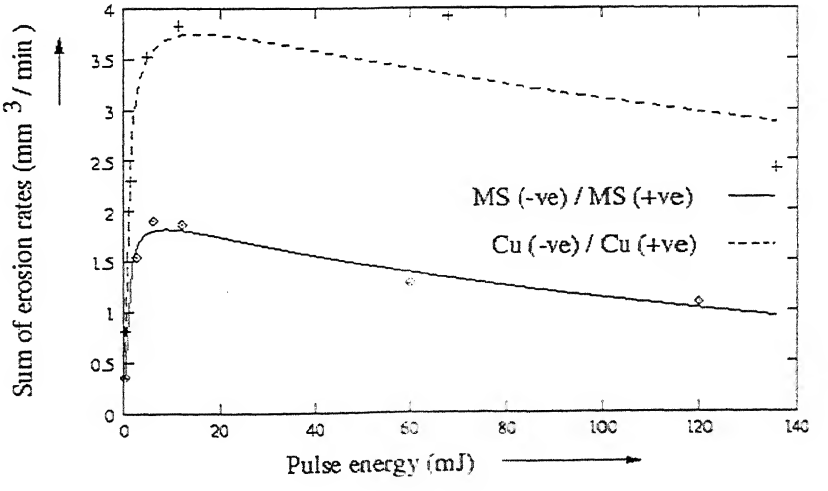

Fig C.4: Sum of erosion rates of similar electrode pair (dielectric: K[illegible]ne)

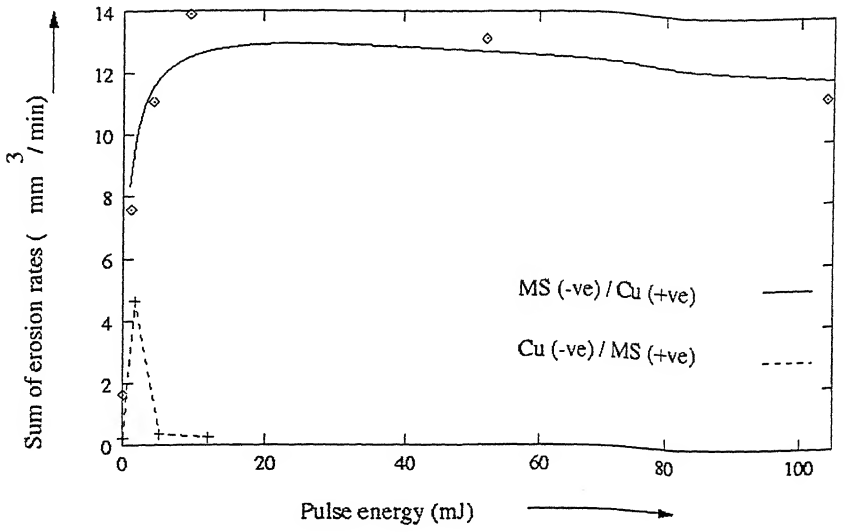

Fig C.4: Sum of erosion rates of dissimilar electrode pair (dielectric: kerosene)

A130908

Date Slip

This book is to be returned on the date last stamped.

A130908